University of Nottingham

UK | CHINA | MALAYSIA

Impacts of Exceptional Points and Phase Angle on the Entanglement Dynamics of Two-Qubit Open Quantum System

H'ng Yee Shean

Supervisor: Dr Tay Buang Ann

Co-supervisor: Dr Toh Sing Poh

August 10, 2025

Thesis submitted in partial fulfillment for the degree of Master of Philosophy

Declaration

I, H'ng Yee Shean, hereby declare that the work presented in this thesis titled *"Impacts of Exceptional Points and Phase Angle on the Entanglement Dynamics of Two-Qubit Open Quantum System"* is my own, except where otherwise acknowledged. This thesis is submitted in partial fulfillment of the requirements for the degree of Master of Philosophy in Department of Mechanical, Materials and Manufacturing Engineering at University of Nottingham Malaysia.

I confirm that this thesis has not been previously submitted, either in whole or in part, for the award of any degree or qualification at this or any other institution. Any contributions from other researchers, collaborators, or sources have been duly cited and acknowledged.

Furthermore, I assert that the research conducted complies with ethical standards and institutional guidelines. All data, results, and interpretations presented herein are accurate to the best of my knowledge.

H'ng Yee Shean
August 10, 2025

Dedication

Dedicated to my secret friend from STPM. Thank you for inspiring me to see physics as a path for my undergraduate studies. Your words made this thesis possible.

"Life is like riding a bicycle. To keep your balance, you must keep moving."

- Albert Einstein

"'And' and 'or' are the basic operations of logic. Together with 'no' (the logical operation of negation) they are a complete set of basic logical operations. All other logical operations, no matter how complex, can be obtained by suitable combinations of these."

- John von Neumann

"A mathematician is a person who can find analogies between theorems; a better mathematician is one who can see analogies between proofs and the best mathematician can notice analogies between theories. One can imagine that the ultimate mathematician is one who can see analogies between analogies."

- Stefan Banach

Acknowledgments

First and foremost, I would like to express my deepest gratitude to my supervisor, Dr. Tay Buang Ann, for his unwavering guidance and invaluable contributions throughout the course of this research. His insightful ideas have consistently provided me with meaningful directions to explore and build upon. While there were times when our perspectives on certain aspects differed, I have come to appreciate how these differing viewpoints created a dynamic and enriching environment for the research. This diversity in thought has greatly helped me develop a more comprehensive approach to structuring my research and crafting this thesis.

I would also like to extend my sincere thanks to my co-supervisor, Dr. Toh Sing Poh, for his valuable support and meticulous reviews during my annual evaluations. His constructive comments and feedback have been instrumental in ensuring the quality and rigor of my work.

Lastly, I am grateful for the support and encouragement I received from my family, friends, and colleagues, whose belief in me has been a constant source of motivation.

To everyone who has contributed to my academic journey, directly or indirectly, thank you. This work would not have been possible without your guidance and encouragement.

Abstract

This study investigates the dynamics of two-qubit systems in open quantum environments, with a focus on the influence of exceptional points (EPs) and phase angle on entanglement dynamics. Two-qubit systems are pivotal in quantum information science, as they are the simplest system that reveals quantum entanglement, a crucial resource for quantum computing and communication. The research explores the effects of coupling, spontaneous emission, and environment on two-qubit states, specifically the X-states, within the framework of the Gorini–Kossakowski–Sudarshan–Lindblad (GKSL) or Lindblad master equation.

EPs are unique to non-Hermitian systems. They affect the system's dynamics significantly when the system approaches EP. Analytical and numerical analyses reveal that third-order EPs occur at specific parameters for two-qubit system, leading to critical changes in eigenvalues and eigenvectors of the Liouvillian superoperator. The study demonstrates that EPs can enhance or suppress entanglement. The concurrence, a quantitative measure of entanglement, peaks around the EPs under certain initial conditions.

Furthermore, the impact of phase angle, θ, that parameterizes the relative phase of maximally entangled states is analyzed. For initial states labeled as $\rho_\Psi(\theta, p)$ in this thesis, the phase angle significantly influences concurrence evolution, enabling tunability of entanglement dynamics. In contrast, for other class of initial states labeled as $\rho_\Phi(\theta, p)$, concurrence exhibits phase invariance, ensuring stability across the variations in θ. Besides this, the analysis shows that the maximum concurrence occurs around EP for some states, the phase angle can also be tuned to increase the concurrence for some initial states. These findings highlight the importance of both EPs and phase angle in optimizing entanglement generation and control.

This research offers valuable insights into the interplay between non-Hermitian physics and quantum entanglement, paving the way for advancements in quantum technologies. The outcomes provide possible practical implications in the field of quantum computation.

Contents

List of Figures

Symbols and Abbreviations

$\|\psi\rangle$	Ket notation of quantum state
$\langle\psi\|$	Bra notation of quantum state
$\vec{r}$	Position vector
$\mathbb{C}$	Complex number set
$\mathbb{R}$	Real number set
σ_1	Pauli matrix, X
σ_2	Pauli matrix, Y
σ_3	Pauli matrix, Z
ρ	Density matrix
I	Identity matrix
U	Unitary matrix
H	Hamiltonian
H_{eff}	Effective Hamiltonian
$\mathcal{L}$	Liouvillian superoperator
σ_-	Lowering operator
σ_+	Raising operator
γ	Spontaneous emission rate of qubit
δ	Detuning
Ω	Swapping coupling between two qubits
Λ	Eigenvalue
$\vec{v}$	Right generalized eigenvector
$\vec{u}$	Left generalized eigenvector
δ_{jk}	Kronecker delta
C	Concurrence
θ	Phase angle
π	Ratio of the circumference of a circle to its diameter
i	Imaginary unit
e	Euler constant

$\mathcal{PT}$	Parity-time
EP	Exceptional point
HEP	Effective Hamiltonian exceptional point
LEP	Liouvillian exceptional point
ESD	Entanglement sudden death
PMEOM	Pseudomode equation of motion
HEOM	Hierarchical equations of motion

List of Publications

B. A. Tay and Y. S. H'ng, "Entanglement generation across exceptional points in two-qubit open quantum system: the role of initial states", accepted by Phys. Rev. E (2025).

Y. S. H'ng and B. A. Tay, "Impacts of local phase on the entanglement dynamics of two-qubit open quantum system", submitted (2025).

Y. S. H'ng and B. A. Tay, "Construction of generalized eigenstates at third-order exceptional points for two-qubit open quantum system", in preparation.

Chapter 1

Introduction

Quantum mechanics has reshaped our understanding of the physical world by revealing phenomena that defy classical intuition. Central to this field are quantum bits, or qubits, which form the basic units of quantum information. The study of qubits and their interactions has become essential due to their potential applications in quantum computing, and quantum communication [1], as well as quantum sensing [2]. This thesis explores the dynamics of one-qubit and two-qubit systems in open quantum environments, with a specific focus on the effect of exceptional point (EP), which play a crucial role in shaping system behavior at its vicinity.

1.1 Background and context

Research into open quantum systems has gained prominence due to its significance in developing robust quantum technologies. These systems interact with external environments, leading to energy dissipation and loss of coherence [3]. To model such interactions, the Gorini–Kossakowski–Sudarshan–Lindblad (GKSL) [4, 5] or Lindblad master equation [6] has emerged as a widely accepted framework. Meanwhile, the concept of EPs, originating from non-Hermitian physics [7–9], has opened new direction for studying quantum systems. EPs occur when eigenvalues and eigenvectors of a system coalesce, resulting in profound changes in system dynamics at its vicinity [10]. These properties have sparked interest in enhancing quantum sensing, photonics, optics and topological energy transfer [11–17].

1.2 Current state of knowledge

The current state of research reveals promising yet incomplete knowledge. For one-qubit systems, EPs have been extensively studied, with theoretical and experimental investigations highlighting their role in quantum sensing and state control [11–17]. In two-qubit systems, research is still ongoing, with experimental

validation [18, 19]. Theoretical models suggest that EPs can influence entanglement dynamics, though they do not always enhance entanglement due to complex system-environment interactions. Physicists are also actively exploring higher-order EPs [14, 20–22] and their connection to entanglement dynamics [23, 24], emphasizing the need for more comprehensive analytical and experimental studies.

1.3 Research questions

This thesis seeks to address the following questions:

1. How do EPs and initial states influence the dynamics of two-qubit systems?
2. Can EPs be used to enhance entanglement in coupled qubit systems?
3. How does phase angle of initial bell's state affect the entanglement dynamics of the system?

1.4 Methodology

The research adopts a mixed-method approach involving eigensystem analysis and numerical simulations. For eigensystem analysis, we will explore the behavior of the system base on eigenvalues and eigenvectors of the system. We will also use computational approach to analytic solution to obtain entanglement dynamics using concurrence [25, 26] as a measure. These multi-faceted approach ensures a comprehensive understanding of how system dynamics evolve.

1.5 Research aim and contributions

The primary aim of this thesis is to explore how EPs shape the behavior of open quantum systems, particularly in two-qubit configurations. One of the key contributions is an in-depth exploration of entanglement behavior near to or away from EPs. Additionally, exploring the impact of phase angle on entanglement behavior will help bridge the gap in existing research on this topic. The research will also provide a method for tuning system parameters to achieve desired outcomes. The last contribution will be expanding knowledge on EPs in two-qubit systems and their technological applications.

1.6 Thesis organization

The thesis is structured in the following way. In chapter 2, we introduce the basic knowledge such as quantum state of qubit and density matrix. we also

introduce the dynamic of one-qubit in open quantum system. Furthermore, we utilize the eigensystem analysis to understand the system dynamics. In chapter 3, we introduce the idea of EP. We also focus on mathematical formulations of EP and system dynamics.

In chapter 4, we introduce the dynamic of two-qubit system and analyze the eigensystem and its EPs. We also introduce the concurrence and the initial state used in the research. In chapter 5, we present numerical findings and analyzes entanglement behavior. In chapter 6, we summarize findings, highlights contributions, and suggests future research directions.

Part I

One-Qubit

Chapter 2

One-qubit in open quantum system

In computing, a bit represents a logical state of either 'true' or 'false', typically denoted as '1' for 'true' and '0' for 'false'. At the classical level, the state of a bit is always definite, regardless of whether we observe it or not. Conversely, at the quantum level, a bit's state is in a superposition of both states until it is observed, and such a bit is referred to as a 'qubit' [1].

One application of qubits is in the field of quantum computing. In 1994, American mathematician Peter Shor developed an algorithm based on qubits to factorize integers, known as Shor's algorithm [27]. Shor's algorithm provides strong evidence of super-polynomial speedup compared to classical algorithms, which could be extremely useful if quantum computers are realized in the future [27].

Another application of qubits is in the field of cryptography. In classical communication, when two parties are exchanging information, a third party can intercept the data without the original parties being aware. However, due to the quantum nature of qubits, any attempt by a third party to intercept the information will disturb the quantum state of the qubits, alerting the two parties to the eavesdropping attempt [28, 29].

The discussion of a two-level system coupled with an environment was initiated by Israel Senitzky in 1963 [30]. In his paper, Senitzky formulated the problem by considering the two-level system as undergoing Brownian motion when interacting with its environment [30]. Consequently, he derived the Langevin equation using Pauli spin matrices [30]. Senitzky later extended the theory by considering a more general type of two-level system and incorporating the effects of a thermal reservoir [31].

Between 1976 and 1978, Vittorio Gorini, Andrzej Kossakowski, George Sudarshan [4, 5], and Göran Lindblad [6] developed the Gorini-Kossakowski-Sudarshan-Lindblad (GKSL) equation, also referred to as the Lindblad master equation or quantum master equation, by assuming the Markovian traits of the quantum system. This breakthrough provided a robust framework applicable to dissipative two-level systems.

2.1 Quantum properties of qubit

A pure state of a qubit is typically defined as

$$|\psi\rangle = \alpha\,|0\rangle + \beta\,|1\rangle\,, \tag{2.1}$$

where $\alpha, \beta \in \mathbb{C}$ and $|\alpha|^2 + |\beta|^2 = 1$. Here, $|0\rangle$ and $|1\rangle$ denote the states '0' and '1', respectively. These states can be expressed in matrix form as

$$|0\rangle = \begin{pmatrix} 1 \\ 0 \end{pmatrix} \qquad \text{and} \qquad |1\rangle = \begin{pmatrix} 0 \\ 1 \end{pmatrix}. \tag{2.2}$$

A mixed state of a qubit is defined as a statistical ensemble of pure states. The density matrix is typically used to describe a mixed state of a qubit given by

$$\rho = \begin{pmatrix} \rho_{11} & \rho_{12} \\ \rho_{21} & \rho_{22} \end{pmatrix}, \tag{2.3}$$

where ρ is a Hermitian positive semi-definite matrix with normalization $\rho_{11} + \rho_{22} = 1$. For a pure state, ρ must satisfy $\mathrm{tr}(\rho^2) = 1$, while for a mixed state, $\mathrm{tr}(\rho^2) < 1$.

There is an elegant way to visualize a qubit in both pure and mixed states. The density matrix for a qubit can be expressed as

$$\rho = \frac{I + \vec{r} \cdot \vec{\sigma}}{2}. \tag{2.4}$$

Here, $\vec{r} = (x, y, z)$ and $\vec{\sigma} = (\sigma_1, \sigma_2, \sigma_3)$ with $\sigma_1, \sigma_2, \sigma_3$ being Pauli matrices. For a pure state, $|\vec{r}| = 1$, while for a mixed state, $|\vec{r}| < 1$. This representation is known as Bloch sphere [32].

2.2 GKSL equation

A system consisting of a qubit coupled with a zero-Kelvin environment and interacting with an electromagnetic field is mathematically described by the optical Bloch equation [33].

Hatano used a simplified version of the system by focusing solely on the oscillating electric field and disregarding the magnetic field [34]. This simplification is described by the GKSL equation, given by

$$\frac{d\rho}{dt} = -i[H, \rho] + \gamma(\sigma_- \rho \sigma_+ - \frac{1}{2}\sigma_+\sigma_-\rho - \frac{1}{2}\rho\sigma_+\sigma_-), \tag{2.5}$$

where the density matrix is

$$\rho(t) = \begin{pmatrix} a(t) & m^*(t) \\ m(t) & b(t) \end{pmatrix}. \tag{2.6}$$

Here, γ denotes the spontaneous emission rate of the qubit. The Hamiltonian of the system is given by

$$H = \begin{pmatrix} -\delta/2 & d \\ d & \delta/2 \end{pmatrix}, \tag{2.7}$$

where d represents the electric field strength, and δ represents the detuning. The equation (2.5) leads to a set of equations given by

$$\frac{da(t)}{dt} = \gamma b(t) - idm(t) + idm^*(t), \tag{2.8}$$
$$\frac{db(t)}{dt} = -\gamma b(t) + idm(t) - idm^*(t), \tag{2.9}$$
$$\frac{dm(t)}{dt} = -ida(t) + idb(t) - (\frac{\gamma}{2} + i\delta)m(t), \tag{2.10}$$
$$\frac{dm^*(t)}{dt} = ida(t) - idb(t) + (-\frac{\gamma}{2} + i\delta)m^*(t). \tag{2.11}$$

These equations have a similar structure to the optical Bloch equation except disregarding the magnetic field. As a result, the Rabi frequency Ω is replaced by the electric field strength d. We obtain a matrix differential equation by vectorizing the density matrix as shown below,

$$\rho = \begin{pmatrix} a(t) & m^*(t) \\ m(t) & b(t) \end{pmatrix} \xrightarrow{\text{vectorization}} \vec{\rho} = \begin{pmatrix} a(t) \\ b(t) \\ m(t) \\ m^*(t) \end{pmatrix}. \tag{2.12}$$

Thus, we have

$$\frac{d}{dt}\begin{pmatrix} a(t) \\ b(t) \\ m(t) \\ m^*(t) \end{pmatrix} = \begin{pmatrix} 0 & \gamma & -id & id \\ 0 & -\gamma & id & -id \\ -id & id & -\frac{\gamma}{2} - i\delta & 0 \\ id & -id & 0 & -\frac{\gamma}{2} + i\delta \end{pmatrix} \begin{pmatrix} a(t) \\ b(t) \\ m(t) \\ m^*(t) \end{pmatrix}. \tag{2.13}$$

This leads to the following equation.

$$\frac{d\vec{\rho}}{dt} = \mathcal{L}\vec{\rho}, \tag{2.14}$$

where

$$\mathcal{L} = \begin{pmatrix} 0 & \gamma & -id & id \\ 0 & -\gamma & id & -id \\ -id & id & -\frac{\gamma}{2} - i\delta & 0 \\ id & -id & 0 & -\frac{\gamma}{2} + i\delta \end{pmatrix}. \tag{2.15}$$

We can further simplify the equation by absorbing γ into the time, t, which is equivalent to letting $\gamma = 1$. In Hatano's paper [34], rather than reducing the

variable γ, he reduced the detuning δ, thereby limiting the possibility of achieving $\delta = 0$. Therefore, we now have

$$\mathcal{L} = \begin{pmatrix} 0 & 1 & -id & id \\ 0 & -1 & id & -id \\ -id & id & -\frac{1}{2} - i\delta & 0 \\ id & -id & 0 & -\frac{1}{2} + i\delta \end{pmatrix}. \tag{2.16}$$

Given the initial state of the system's density matrix, the time evolution of density matrix given in equation (2.14) can be computed and represented by a parametric curve $\vec{r}$ in Bloch sphere given in equation (2.4).

2.3 Eigensystem

To understand the dynamics of the system, we analyze the eigensystem of the matrix $\mathcal{L}$. The characteristic polynomial of $\mathcal{L}$ is given by $f(\Lambda) = \det(\mathcal{L} - I\Lambda)$, where

$$f(\Lambda) = \Lambda^4 + 2\Lambda^3 + \frac{1}{4}\Lambda^2(5 + 16d^2 + 4\delta^2) + \frac{1}{4}\Lambda(1 + 4\delta^2 + 8d^2). \tag{2.17}$$

The eigenvalues are given by the root of the characteristic polynomial. Solving $f(\Lambda) = 0$, we have

$$\Lambda_1 = 0, \tag{2.18}$$

$$\Lambda_2 = -\left(\frac{2}{3} + u + s\right), \tag{2.19}$$

$$\Lambda_3 = -\left(\frac{2}{3} + u \cdot e^{2\pi i/3} + s \cdot e^{-2\pi i/3}\right), \tag{2.20}$$

$$\Lambda_4 = -\left(\frac{2}{3} + u \cdot e^{-2\pi i/3} + s \cdot e^{2\pi i/3}\right), \tag{2.21}$$

where

$$u = \sqrt[3]{q + \sqrt{p^3 + q^2}}, \tag{2.22}$$

$$s = \sqrt[3]{q - \sqrt{p^3 + q^2}}, \tag{2.23}$$

and

$$p = \frac{1}{3}\left(\delta^2 + 4d^2 - \frac{1}{12}\right), \tag{2.24}$$

$$q = \frac{1}{6}\left(\delta^2 - 2d^2 + \frac{1}{36}\right). \tag{2.25}$$

For $\Lambda_1 = 0$, we can solve for its corresponding eigenvector,

$$\vec{v_1} = \begin{pmatrix} a_1 \\ b_1 \\ m_1 \\ m_1^* \end{pmatrix}. \tag{2.26}$$

Since $(\mathcal{L} - I\Lambda_1)\vec{v_1} = 0$ and $\Lambda_1 = 0$, we have

$$\begin{pmatrix} 0 & 1 & -id & id \\ 0 & -1 & id & -id \\ -id & id & -\frac{1}{2} - i\delta & 0 \\ id & -id & 0 & -\frac{1}{2} + i\delta \end{pmatrix} \begin{pmatrix} a_1 \\ b_1 \\ m_1 \\ m_1^* \end{pmatrix} = \begin{pmatrix} 0 \\ 0 \\ 0 \\ 0 \end{pmatrix}. \tag{2.27}$$

Using Gaussian elimination, we obtain

$$a_1 = N_1, \tag{2.28}$$

$$b_1 = \frac{4N_1 d^2}{4d^2 + 4\delta^2 + 1}, \tag{2.29}$$

$$m_1 = -\frac{2dN_1}{4d^2 + 4\delta^2 + 1}(2\delta + i), \tag{2.30}$$

$$m_1^* = -\frac{2dN_1}{4d^2 + 4\delta^2 + 1}(2\delta - i). \tag{2.31}$$

where N_1 is a normalization constant. Since eigenvalue $\Lambda_1 = 0$ corresponds to equilibrium point of the system, its eigenvector must satisfy the trace condition of density matrix, $\mathrm{tr}(\rho) = 1$, or $(v_1)_{00} + (v_1)_{11} = 1$. This gives

$$N_1 = \frac{4d^2 + 4\delta^2 + 1}{8d^2 + 4\delta^2 + 1}, \tag{2.32}$$

and $\vec{v_1}$ takes a simpler form

$$\vec{v_1} = \frac{1}{8d^2 + 4\delta^2 + 1} \begin{pmatrix} 4\delta^2 + 4d^2 + 1 \\ 4d^2 \\ -2d(2\delta + i) \\ -2d(2\delta - i) \end{pmatrix}. \tag{2.33}$$

We can express the equilibrium state in terms of Bloch sphere components, x_{eq}, y_{eq} and z_{eq} given by

$$x_{\mathrm{eq}} = -\frac{8d\delta}{8d^2 + 4\delta^2 + 1}, \tag{2.34}$$

$$y_{\mathrm{eq}} = -\frac{4d}{8d^2 + 4\delta^2 + 1}, \tag{2.35}$$

$$z_{\mathrm{eq}} = \frac{1}{8d^2 + 4\delta^2 + 1}(4\delta^2 + 1). \tag{2.36}$$

Next, we solve $(\mathcal{L} - I\Lambda_k)\vec{v}_k = 0$ for corresponding eigenvectors, $\vec{v}_k$, where $k = 2, 3, 4$. Using a similar notation to $\vec{v}_1$ given by equation (2.26), we can solve for the components of $\vec{v}_k$. They are

$$a_k = 2d(1 + 2\Lambda_k)N_k, \tag{2.37}$$
$$b_k = -2d(1 + 2\Lambda_k)N_k, \tag{2.38}$$
$$m_k = (1 + \Lambda_k)[2\delta + i(1 + 2\Lambda_k)]N_k, \tag{2.39}$$
$$m_k^* = (1 + \Lambda_k)[2\delta - i(1 + 2\Lambda_k)]N_k. \tag{2.40}$$

Then, we have

$$\vec{v}_k = N_k \begin{pmatrix} 2d(1 + 2\Lambda_k) \\ -2d(1 + 2\Lambda_k) \\ (1 + \Lambda_k)[2\delta + i(1 + 2\Lambda_k)] \\ (1 + \Lambda_k)[2\delta - i(1 + 2\Lambda_k)] \end{pmatrix}, \tag{2.41}$$

for $k = 2, 3, 4$. For the sake of completeness, we can also find out the left eigenvectors. By solving eigenvector equations $\mathcal{L}^\dagger \vec{u}_1 = 0$ and $(\mathcal{L}^\dagger - \Lambda_j^* I)\vec{u}_j = 0$ for $j = 2, 3, 4$, the left eigenvectors are given by

$$\vec{u}_1 = \begin{pmatrix} 1 \\ 1 \\ 0 \\ 0 \end{pmatrix} \tag{2.42}$$

and

$$\vec{u}_j = \begin{pmatrix} (1 + 2\Lambda_j^*)[4\delta^2 + (1 + 2\Lambda_j^*)^2] \\ (1 - 2\Lambda_j^*)[4\delta^2 + (1 + 2\Lambda_j^*)^2] \\ -4d\Lambda_j^*[2\delta - i(1 + 2\Lambda_j^*)] \\ -4d\Lambda_j^*[2\delta + i(1 + 2\Lambda_j^*)] \end{pmatrix}, \tag{2.43}$$

where $j = 2, 3, 4$. Applying biorthogonal condition of left and right eigenvectors, given by $\vec{u}_j^\dagger \vec{v}_k = \delta_{jk}$, where $\dagger$ is matrix transpose conjugate. The normalizing coefficient N_k can be computed as

$$N_k = \frac{1}{4d\Lambda_k((2\Lambda_k + 1)^2(4\Lambda_k + 3) - 4\delta^2)}. \tag{2.44}$$

Computing the system's dynamics does not necessitate the use of both left and right eigenvectors. The left eigenvectors are included primarily to provide a complete mathematical formulation.

In the biorthogonal formalism, the sets of right and left generalized eigenvectors are constructed such that they satisfy the biorthogonal relation $\vec{u}_j^\dagger \vec{v}_k = \delta_{jk}$. Here, the left eigenvectors $\vec{u}_j$ form the dual basis to the right eigenvectors $\vec{v}_k$. This relation ensures that each $\vec{u}_j$ acts as a linear functional that extracts the coefficient

of its corresponding $\vec{v}_k$. Such a construction guarantees completeness and provides a natural projection mechanism in the non-Hermitian matrices [35].

By analyzing the eigensystem of the matrix, we will later demonstrate that the system can be categorized into four cases, they are the overdamped, underdamped and critically damped region at a second-order EP and third-order EP.

Chapter 3

Exceptional points for one-qubit

Research on the EP in non-Hermitian quantum mechanics began approximately two decades ago when it challenged the traditional assumption that a Hamiltonian must be Hermitian to have real eigenvalues. However, studies demonstrated that an operator does not need to be Hermitian to exhibit real eigenvalues; operators that are $\mathcal{PT}$-symmetric can also have real, positive-definite eigenvalues [36]. The research also showed that $\mathcal{PT}$-symmetry can break, causing some real eigenvalues to split into complex pairs [36]. This point of symmetry breaking is now known as the EP.

The rigorous analysis on EP in an open quantum system was studied in 1997 and 1998 [37, 38]. To properly describe the open quantum system in terms of state vector, effective Hamiltonian, usually non-Hermitian, must be used to describe the system. The dissipative nature of the open quantum system arise from the complex eigenvalues of effective Hamiltonian, where imaginary part of the eigenvalues signifies the decay channel and real part represents the oscillatory behavior of the system [38]. An EP occurs when two complex conjugate eigenvalues and their corresponding eigenvectors coalesce, indicating a phase transition in the open quantum system [38].

Between 2006 and 2024, the EP exhibited by the Liouvillian superoperator in the GKSL equation began to attract significant attention [34, 39–43]. This interest is primarily due to the fact that the effective Hamiltonian approach for describing open quantum systems does not account for quantum jumps [44]. Just like effective non-Hermitian Hamiltonian, the Liouvillian superoperator has complex eigenvalues, where the real part represents decay channels and the imaginary part represents the oscillatory behavior of the system [45]. We can denote the EPs described by the effective Hamiltonian as HEP, and those described by the Liouvillian superoperator as LEP.

The study of EP has become increasingly popular among physicists because of its broad applications in the sensor industry. One such application is in frequency and energy splitting detection by sensors. Research indicates that the sensitivity of a sensor can be enhanced by operating it at its EP [46]. Following this discovery, physicists developed a general theory for sensor enhancement at EPs [47].

Since around 2015, numerous studies have been conducted on sensor enhancement technologies utilizing EP [11–17].

Another application of EPs is in optics and photonics. A study by Miri and Alù demonstrates the potential to achieve a variety of exotic optical functionalities associated with EP by manipulating dissipation and amplification within a nanophotonic system [48]. These functionalities include ultrasensitive measurements, control over the modal content of multimode lasers, and adiabatic control of topological energy transfer for mode and polarization conversion [48]. Additionally, research on EPs helps confirm the feasibility of realizing non-Hermitian light transport [49]. This finding could contribute to the development of a new generation of free-space optical communication devices [49].

3.1 Theory of exceptional point

A Hermitian matrix is always diagonalizable. However, not all diagonalizable matrices are Hermitian. For instance, a unitary matrix, which is not necessarily Hermitian, can also be diagonalizable. A diagonalizable matrix, A, can be transformed into a diagonal matrix, D, through a change of basis

$$D = \begin{pmatrix} \lambda_1 & 0 \\ 0 & \lambda_2 \end{pmatrix}, \tag{3.1}$$

where λ_1, λ_2 are eigenvalues of matrix A. In any system, degeneracy occurs when two or more eigenvalues coalesce. In a Hermitian system, degeneracy arises when the matrix can be diagonalized as

$$A = \begin{pmatrix} \lambda & 0 \\ 0 & \lambda \end{pmatrix}. \tag{3.2}$$

In this case, the eigenvectors remain orthogonal despite the coalescence of eigenvalues. However, a special type of degeneracy exists in non-Hermitian systems, where diagonalization is not possible. Instead, the matrix can at most be transformed into a Jordan block form [50, 51], given by

$$B = \begin{pmatrix} \lambda & 1 \\ 0 & \lambda \end{pmatrix}. \tag{3.3}$$

The parameters leading to this form of degeneracy are known as EP. At an EP, two or more eigenvalues, along with their corresponding eigenvectors, coalesce. For non-Hermitian system where two eigenvectors coalesce at the EP, a generalized eigenvector $\vec{v}^{(1)}$ [50, 52] must be introduced to replace the missing eigenvector through a generalized eigenvalue equation

$$(A - \lambda I)\vec{v}^{(1)} = \vec{v}, \tag{3.4}$$

where $\vec{v}$ is an eigenvector of A. When p eigenvalues coalesce at an EP, it is called a pth-order EP. The generalized eigenvectors are computed using a set of equations known as the Jordan chain [50], given by

$$\vec{v}^{(m-2)} = (A - \lambda I)\vec{v}^{(m-1)}, \tag{3.5}$$
$$\vec{v}^{(m-3)} = (A - \lambda I)\vec{v}^{(m-2)}, \tag{3.6}$$
$$\vdots$$
$$\vec{v} = (A - \lambda I)\vec{v}^{(1)}, \tag{3.7}$$

where $\vec{v}, \vec{v}^{(1)}, ..., \vec{v}^{(m-2)}, \vec{v}^{(m-1)}$ are the generalized eigenvectors of matrix A.

3.2 Exceptional points of the system

Previously, we have expressed the eigenvectors of Lindblad operator in terms of their corresponding eigenvalues. Specifically, $\vec{v}_2, \vec{v}_3, \vec{v}_4$ in equation (2.41), share a common structure as functions of the eigenvalues. We observed that when two or more of the eigenvalues $\Lambda_2, \Lambda_3, \Lambda_4$ coalesce, the eigenvectors $\vec{v}_2, \vec{v}_3, \vec{v}_4$ also coalesce.

As stated in Reference [34], there exist second- and third-order EPs for $\mathcal{L}$. These EPs can be determined by equating Λ_3 and Λ_4, which translates to solving the equation $p^3 + q^2 = 0$. To make the analysis simpler, we define

$$\eta \equiv \frac{d}{\sqrt{2}\delta}. \tag{3.8}$$

Solving $p^3 + q^2 = 0$ results in the following expression,

$$\delta_\pm = \frac{1}{2}\sqrt{\frac{1}{8\eta^4 + 20\eta^2 \pm 8\sqrt{\eta^2(\eta^2-1)^3} - 1}}. \tag{3.9}$$

We can visualize the parameter space by plotting δ against η when the matrix $\mathcal{L}$ is at an EP. Figure 3.1 illustrates the relationship between δ and η in the parameter space.

At a second-order EP, the vectors $\vec{v}_3$ and $\vec{v}_4$ coincide, as depicted along the red curves in Figure 3.1 [34]. For third-order EPs, the vectors $\vec{v}_2, \vec{v}_3$, and $\vec{v}_4$ precisely converge at $\delta = \frac{1}{6\sqrt{3}}$ and $\eta = 1$ [34] as shown in Figure 3.1. Both second and third-order EPs signify a state of critical damping. In the shaded region of Figure 3.1, where $p^3 + q^2 < 0$, all eigenvalues are real, indicating that the system is in the overdamped region. Conversely, in the unshaded region, where $p^3 + q^2 > 0$, Λ_1 and Λ_2 are real, while Λ_3 and Λ_4 take the form $\Lambda_3 = \lambda + i\omega$ and $\Lambda_4 = \lambda - i\omega$, with λ and ω being real numbers. This configuration characterizes an underdamped system.

To understand how eigenvalues change within the parameter space of δ versus η, we can visualize Λ by fixing the detuning δ. For example, by fixing $\delta = 0.05$, we

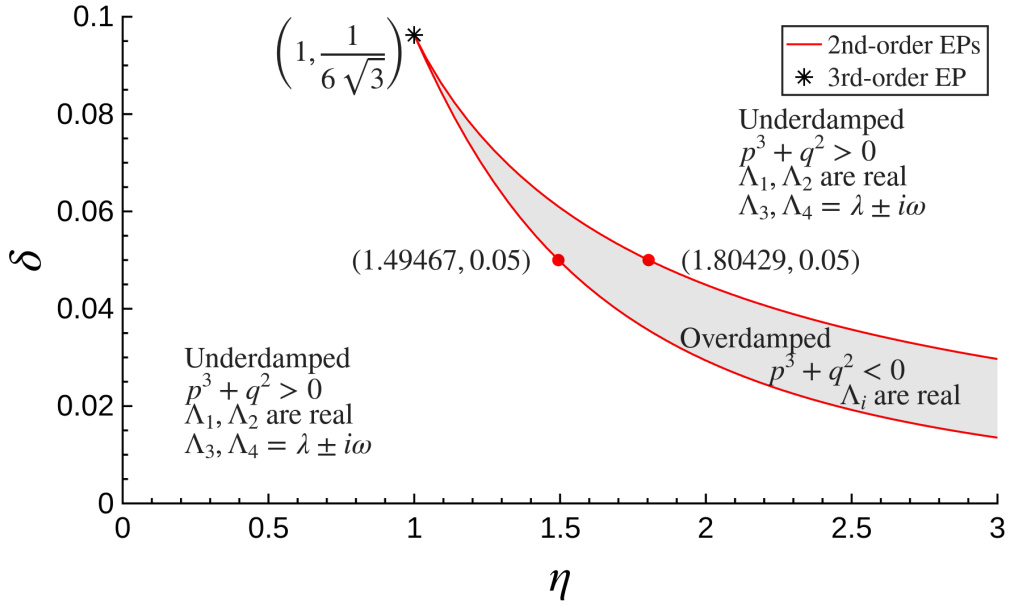

Figure 3.1: Parameter space δ vs η

can plot the real and imaginary parts of Λ vs δ as shown in Figure 3.2. Alongside the real and complex eigenvalues of the graph, we observe two eigenvalues converging at the approximate values of $\eta = 1.49467$ and $\eta = 1.80429$, representing second-order EPs and resulting in the matrix $\mathcal{L}$ being non-diagonalizable. Graphically, it is evident that in the underdamped region, Λ_1 and Λ_2 are real numbers, and Λ_3 and Λ_4 are complex conjugates, while all eigenvalues are real numbers in the overdamped region.

We use blue and green curves in the underdamped region to avoid ambiguity and make it easier to distinguish the pairing of real and imaginary parts of the eigenvalues. This is because in the underdamped region the real and imaginary parts are separated. In contrast, the overdamped region does not have this issue as the imaginary part of all eigenvalues is zero.

3.3 Generalized eigenvectors

At a second-order EP, two eigenvalues and eigenvectors coalesce, only three sets of eigenvalues, $\Lambda_1, \Lambda_2, \Lambda_3$ and their corresponding eigenvectors, $\vec{v}_1, \vec{v}_2, \vec{v}_3$ for the Lindblad superoperator $\mathcal{L}$ can be identified. The eigenvalues at second-order EPs

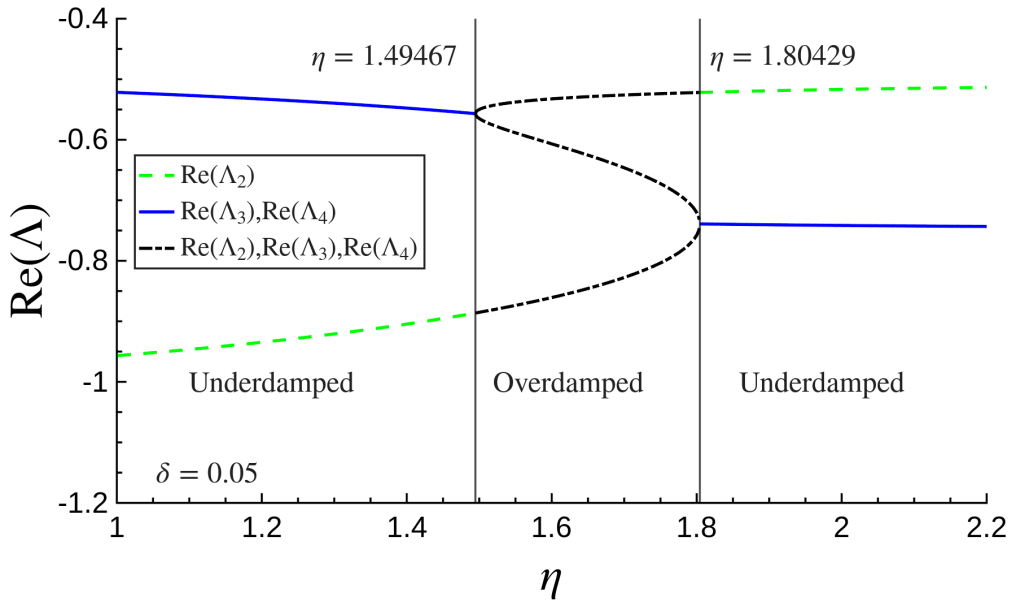

(a)

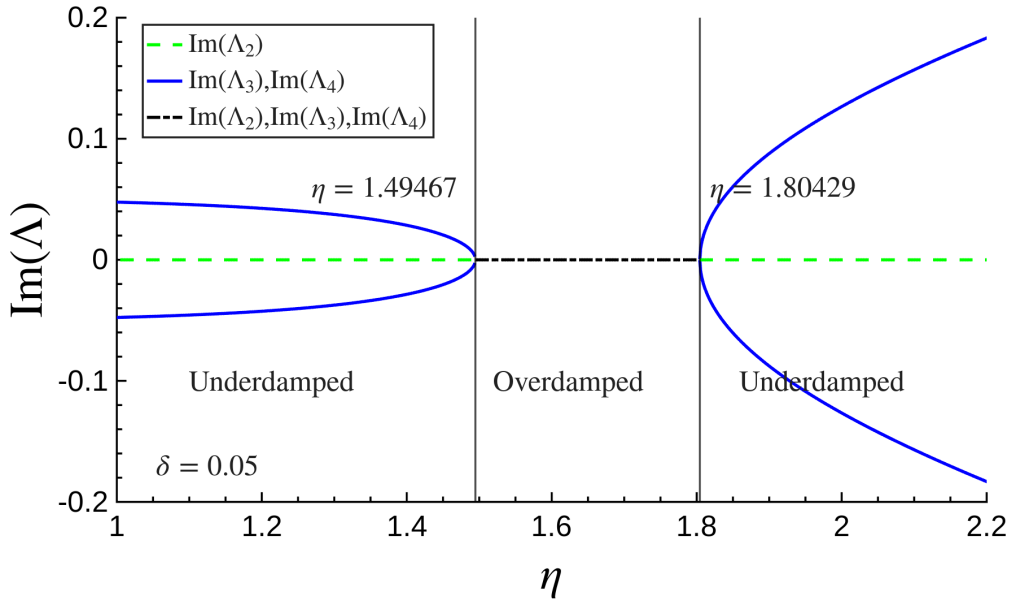

(b)

Figure 3.2: (a) Re(Λ) vs. η and (b) Im(Λ) vs. η. Lines with the same style in both plots correspond to the real and imaginary parts of the same complex eigenvalue. The parameter δ is fixed at 0.05.

are given by

$$\Lambda_1 = 0, \tag{3.10}$$

$$\Lambda_2 = -\left(\frac{2}{3} + 2u\right), \tag{3.11}$$

$$\Lambda_3 = -\left(\frac{2}{3} - u\right), \tag{3.12}$$

where

$$u = \sqrt[3]{q} \tag{3.13}$$

and

$$q = \frac{1}{6}\left(\delta^2 - 2d^2 + \frac{1}{36}\right). \tag{3.14}$$

Mathematically, these eigenvectors are considered a special type of generalized eigenvectors. In the case of a non-diagonalizable matrix $\mathcal{L}$ at a second-order EP, there exists four generalized eigenvectors $\vec{v}_1, \vec{v}_2, \vec{v}_3, \vec{v}_4$ that satisfies the following equation

$$(\mathcal{L} - \Lambda_1 I)\vec{v}_1 = 0, \tag{3.15}$$

$$(\mathcal{L} - \Lambda_2 I)\vec{v}_2 = 0, \tag{3.16}$$

$$(\mathcal{L} - \Lambda_3 I)\vec{v}_3 = 0, \tag{3.17}$$

$$(\mathcal{L} - \Lambda_3 I)\vec{v}_4 = \vec{v}_3. \tag{3.18}$$

The corresponding left generalized eigenvectors, obtained from the adjoint matrix $\mathcal{L}^\dagger$, satisfy

$$(\mathcal{L}^\dagger - \Lambda_1^* I)\vec{u}_1 = 0, \tag{3.19}$$

$$(\mathcal{L}^\dagger - \Lambda_2^* I)\vec{u}_2 = 0, \tag{3.20}$$

$$(\mathcal{L}^\dagger - \Lambda_3^* I)\vec{u}_4 = 0, \tag{3.21}$$

$$(\mathcal{L}^\dagger - \Lambda_3^* I)\vec{u}_3 = \vec{u}_4. \tag{3.22}$$

Here, the ordering of the left eigenvectors $\vec{u}_j$ is deliberately chosen so that the biorthogonality condition, $\vec{u}_j^\dagger \vec{v}_k = \delta_{jk}$, is satisfied. The complete expression for left and right generalized eigenvectors for second-order EP can be found in Appendix A.1.

Following the similar pattern, at a third-order EP, three eigenvalues and eigenvectors coalesce. The eigenvalues at third-order EP are given by

$$\Lambda_1 = 0, \tag{3.23}$$

$$\Lambda_2 = -\frac{2}{3}. \tag{3.24}$$

Consequently, there exists four generalized eigenvector $\vec{v}_1, \vec{v}_2, \vec{v}_3, \vec{v}_4$ that satisfies the following equation

$$(\mathcal{L} - \Lambda_1 I)\vec{v}_1 = 0, \tag{3.25}$$
$$(\mathcal{L} - \Lambda_2 I)\vec{v}_2 = 0, \tag{3.26}$$
$$(\mathcal{L} - \Lambda_2 I)\vec{v}_3 = \vec{v}_2, \tag{3.27}$$
$$(\mathcal{L} - \Lambda_2 I)\vec{v}_4 = \vec{v}_3. \tag{3.28}$$

To complete the analysis, the left generalized eigenvectors can be solved by following

$$(\mathcal{L}^\dagger - \Lambda_1^* I)\vec{u}_1 = 0, \tag{3.29}$$
$$(\mathcal{L}^\dagger - \Lambda_2^* I)\vec{u}_4 = 0, \tag{3.30}$$
$$(\mathcal{L}^\dagger - \Lambda_2^* I)\vec{u}_3 = \vec{u}_4, \tag{3.31}$$
$$(\mathcal{L}^\dagger - \Lambda_2^* I)\vec{u}_2 = \vec{u}_3. \tag{3.32}$$

Again, the ordering of the left eigenvectors $\vec{u}_j$ is deliberately chosen so that the biorthogonality condition $\vec{u}_j^\dagger \vec{v}_k = \delta_{jk}$ is satisfied. The complete expression for left and right generalized eigenvectors for second-order EP can be found in Appendix A.2.

3.4 Dynamics of the system

In this section, we will discuss the dynamics of overdamped, underdamped, and critically damped systems. Since we have a detuning parameter, δ, it simplifies our analysis to fix its value at $\delta = 0.05$, where the second-order EPs occur at $\eta = 1.495$ and $\eta = 1.804$ (cf. Figure 3.1). For the initial condition, the system will start in the state $|1\rangle$, where $x(0) = y(0) = 0$ and $z(0) = -1$.

In the case of the underdamped system, we set $\eta = 1$ to tackle underdamped region before second-order EP at $\eta = 1.495$. Figure 3.3(a) shows the components of the Bloch sphere over time for the underdamped system. Although the system is in the underdamped regime, the oscillation is not prominent. This is because η, which is proportional to the electric field parameter d shown in equation (3.8), governs the frequency of oscillation. From Figure 3.2(b), we observe that the imaginary parts of the eigenvalues Λ_3 and Λ_4 are small and remain nearly constant close to 0.05, the time period is around $T \approx 1/0.05 \approx 20$ for $\eta < 1.495$, where $\eta = 1.495$ is second-order EP acting as boundary between underdamped and overdamped region. As a result, the oscillations in the system are small. Additionally, the purity of the system, denoted by r, approaches an equilibrium value close to 1, indicating that the system approaches a pure state at equilibrium.

Figure 3.3(b) illustrates the underdamped regime when $\eta = 10$, which falls within the range of $\eta > 1.804$, where $\eta = 1.804$ is another second-order EP acting as boundary between overdamped and underdamped region. As shown in Figure

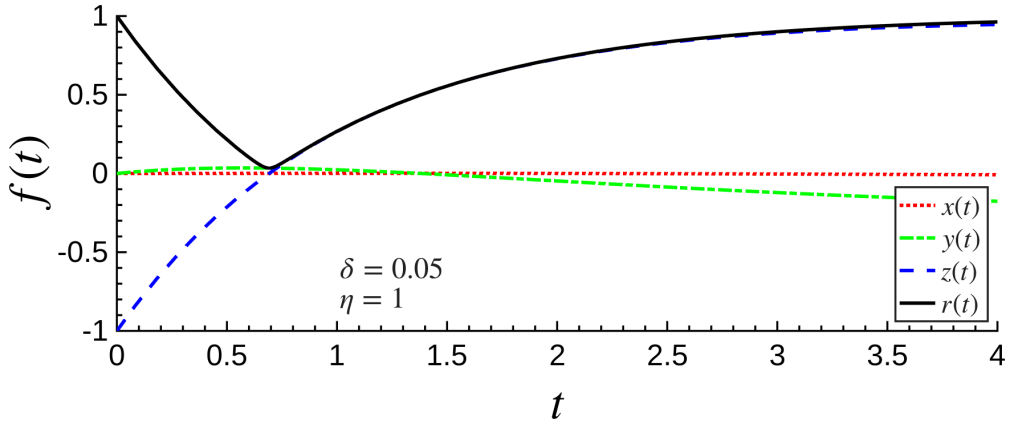

(a)

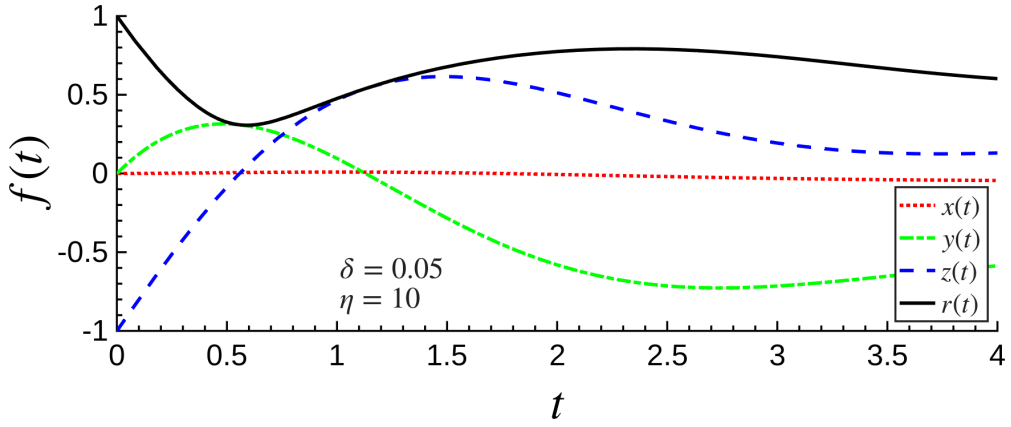

(b)

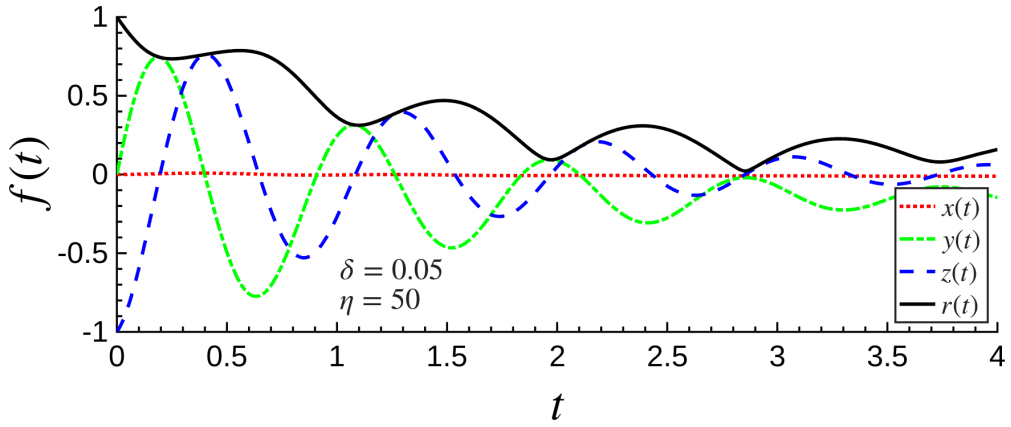

(c)

Figure 3.3: Graphs showing the Bloch components $x(t)$, $y(t)$, $z(t)$, and $r(t)$, represented by the red, green, blue, and black curves, respectively by fixing $\delta = 0.05$ and a few η. (a) $\eta = 1$. System is in underdamp region for $\eta < 1.495$. (b) $\eta = 10$. System is in underdamp region for $\eta > 1.804$. (c) $\eta = 50$. System is in underdamp region for $\eta > 1.804$.

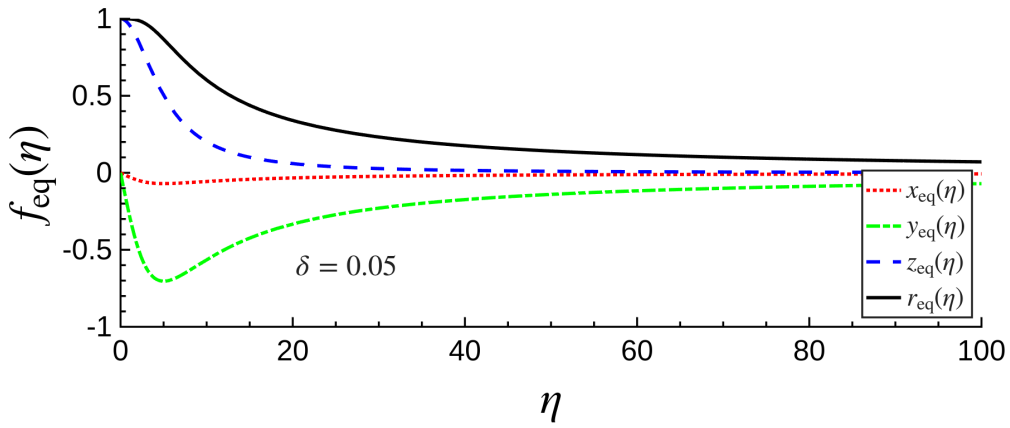

Figure 3.4: Graph of equilibrium point, $x_{\text{eq}}(\eta), y_{\text{eq}}(\eta), z_{\text{eq}}(\eta), r_{\text{eq}}(\eta)$ vs η with fix parameter of $\delta = 0.05$.

3.2(b), the imaginary part of the eigenvalues Λ_3 and Λ_4 increases as η increases, making the oscillations more pronounced compared to when $\eta = 1$. Additionally, the equilibrium value of the system's purity is lower than in the case where $\eta = 1$.

As we increase η further to 50, the frequency of oscillations continues to rise, and the system's equilibrium purity approaches zero, as seen in Figure 3.3(c). This shows how the electric field strength d, proportional to η, determines the equilibrium state. Figure 3.4 clearly demonstrates that as the electric field dominates, the equilibrium point of the Bloch components approaches zero. This indicates that a stronger electric field leads to a more mixed state, as also reflected in Figure 3.4.

At $\eta = 1.495, 1.804$, the system reaches the critical damped region, also known as second-order EP. Similar to classical harmonic oscillator, the damping of the system is just enough to stop the oscillation as shown in Figure 3.5(a) and 3.5(c). We can see that the oscillating trait vanishes, each component of Bloch sphere goes to equilibrium quickly. Similarly, overdamped system occur when $1.495 < \eta < 1.804$, shown in Figure 3.5(b), with $\eta = 1.6$. For third-order EP, three eigenvalues and eigenvectors coalesce at $\eta = 1$ and $\delta = 1/6\sqrt{3}$. The dynamics is shown in Figure 3.6.

3.5 Discussion

We begin by noting that the one-qubit system under study exhibits two types of EPs, second-order EPs and a third-order EP. In regions where $\delta < 1$, the system can traverse two second-order EPs by tuning electric field. This is illustrated in Figure 3.1, where the system effectively undergoes two dynamical phase transitions. In contrast, when $\delta > 1$, the system does not encounter any EPs and maintains persistent oscillatory behavior throughout its evolution. Additionally, at the third-order EP $\delta = 1$, the system passes through a single third-order EP,

also depicted in Figure 3.1.

Unlike many previous studies on EPs, the dynamical phase transitions observed here are relatively subtle, see Figure 3.5 and 3.6. This is primarily because the EPs in our system emerge at lower values of the parameter η, which corresponds to the external electric field strength. At low electric field strength, oscillatory behavior is inherently suppressed. As a result, the exotic features commonly associated with EPs in other works [11–17], such as abrupt transitions or dramatic enhancements are less pronounced in our setup.

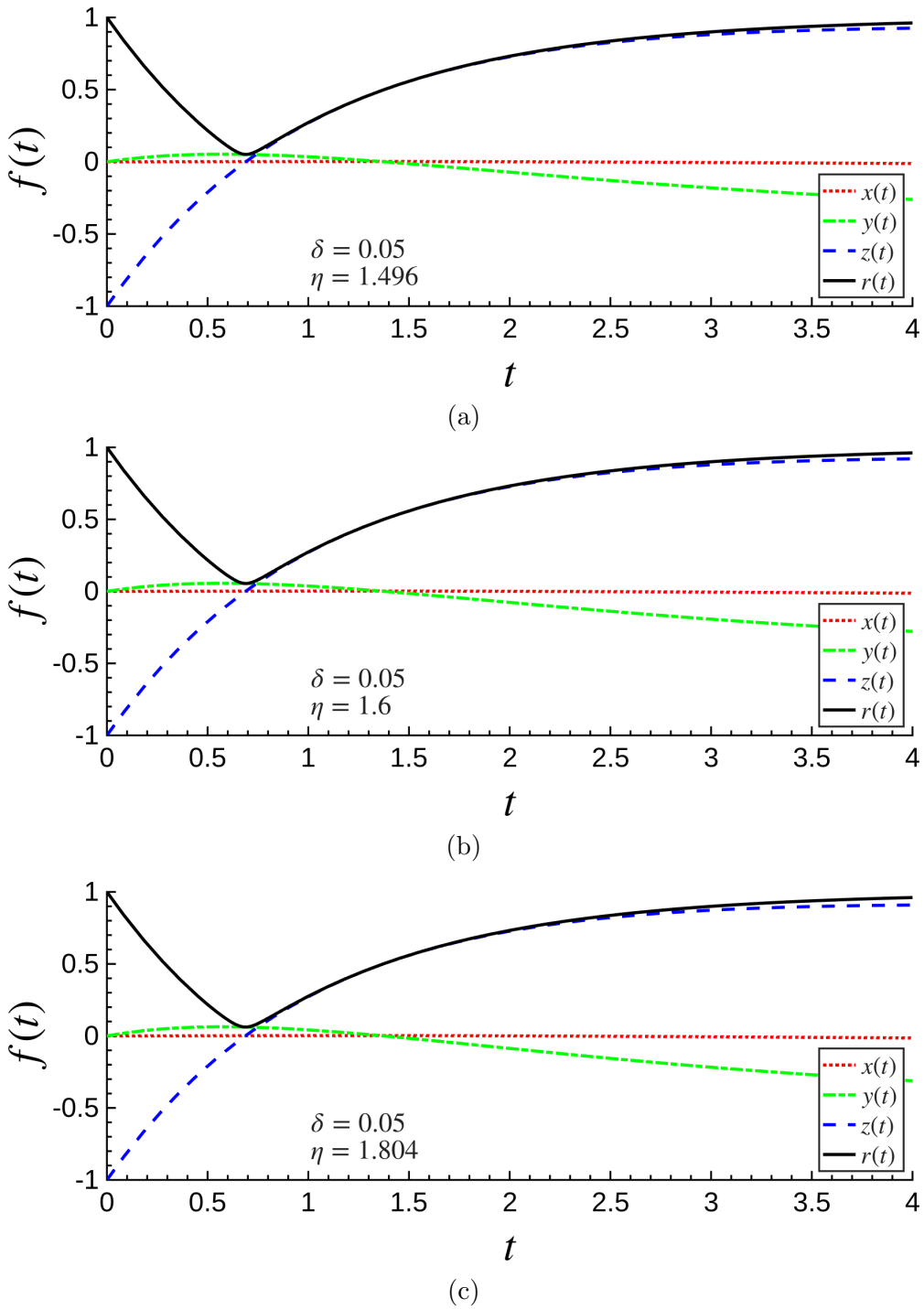

Figure 3.5: Graphs showing the Bloch components $x(t)$, $y(t)$, $z(t)$, and $r(t)$, represented by the red, green, blue, and black curves, respectively by fixing $\delta = 0.05$ and η varied. (a) $\eta = 1.495$. System is at second-order EP. (b) $\eta = 1.6$. System is in overdamping region. (c) $\eta = 1.804$. System is at another second-order EP.

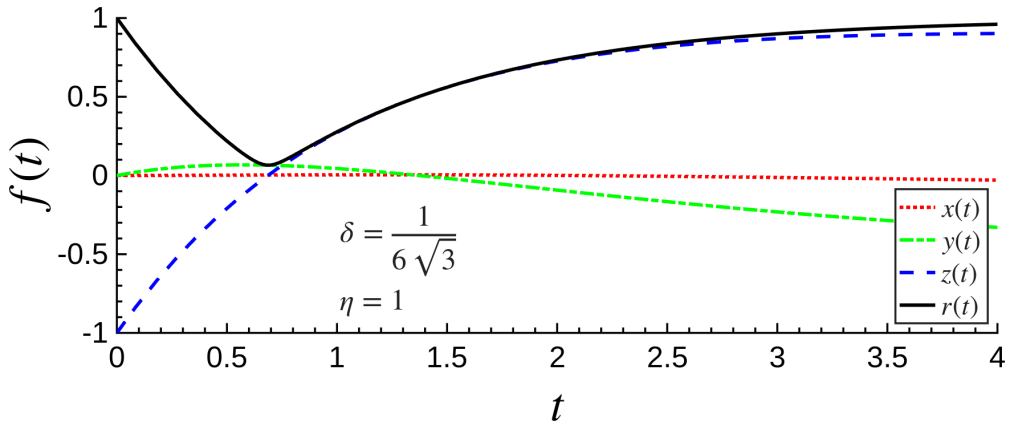

Figure 3.6: Graph of Bloch components, $x(t), y(t), z(t), r(t)$ vs time, t. The system is at third-order EP with parameters $\delta = 1/6\sqrt{3}$ and $\eta = 1$.

Part II

Two-Qubit

Chapter 4

Two-qubit in open quantum system

Aside from the one-qubit case, EPs also play a significant role in two-qubit open quantum systems. Recent developments in quantum sensing have extended into the two-qubit regime, offering new insights into EP-engineered quantum effects. These effects can be harnessed in applications involving non-Hermitian quantum devices [53]. Moreover, studies have demonstrated that multiqubit sensing at EPs is feasible through a Floquet driving scheme that induces effective multibody Ising-type interactions [54]. This approach can be experimentally implemented using trapped ions or superconducting qubits [54].

Beyond quantum sensing, theoretical progress has also been made in understanding EPs in two-qubit open quantum systems. A specific type of EP, known as a hidden EP, has been identified through the insertion of a counting field into the Lindbladian. It has been shown that such hidden EPs are experimentally accessible using platforms like superconducting qubits, Rydberg atoms, and trapped ions [55]. Additionally, recent work has shown that the fastest relaxation to the steady state takes place on so-called LEP manifolds, which are associated with the transition to an effective Zeno regime [56].

4.1 Entanglement dynamics in two-qubit system

In realistic two-qubit systems, entanglement between the qubits inevitably degrades due to interactions with the surrounding environment. Overcoming this challenge is essential for building practical quantum computers. The dynamics of entanglement in two-qubit systems have been extensively studied by physicists since the late 20th century and early 21st century [57–69].

Research has shown that for all two-qubit Werner states in a zero-Kelvin environment, the system's concurrence, a measure of entanglement, decays to zero in finite time [70, 71]. This phenomenon is known as entanglement sudden death (ESD). However, the study proposed a method to extend the time before ESD

occurs by applying specific local operations to the initial state [70].

Further investigation by Ali et al. [72] found that all initial, non-interacting two qubits X-states experience ESD in a thermal reservoir, while some X-states may avoid ESD in a zero-Kelvin environment. The study also demonstrated that, similar to the zero-Kelvin case, ESD in a thermal reservoir can be delayed by applying appropriate local operations to the initial state [72]. Another study by An, Wang, and Luo [73] examined two interacting qubits within a common environment. Their research highlights the dual role of the environment in influencing qubits entanglement. The first role involves the degradation of entanglement due to coherent dipole-dipole interactions [73]. Conversely, the second role demonstrates that the environment can also create stable entanglement in qubits prepared initially in a separable state [73].

Chakraborty and Sarma [24] conducted one of the first studies on entanglement near EPs in 2017. Their findings showed that delaying ESD is possible near EPs in binary and ternary mechanical $\mathcal{PT}$-symmetric systems. Kumar et al. [74] further explored this area, revealing that a system with a specific type of time-periodic Hamiltonian could cause a non-entangled state evolves into a maximally entangled state at an EP. Similarly, Li et al. [23] demonstrated that entanglement generation speeds up near EPs in two coupled driven non-Hermitian qubits. These studies suggest that EPs could significantly influence entanglement dynamics.

Another aspect of two-qubit open quantum systems is the limited research involving initial maximally entangled states with phase angle. The only notable study utilizing phase angle in a two-qubit open quantum system was conducted by Daryanoosh et al. on optical cavities and two-level atoms [75]. Exploring the role of phase angle in maximally entangled states convexly combine with maximally mixed state, known as Werner state [76–78], will also be a key focus of this research. Moreover, Du et al. [79] demonstrated that the quantum mechanical phase of a maximally entangled state can be experimentally observed. In addition, studies by Liu et al. [80] and Jiang et al. [81] have shown that the Werner state can be experimentally prepared in the laboratory. These findings further support the exploratory value of the theoretical investigation presented in this research.

4.2 Two-qubit Coupling

We consider a system where two qubits, namely qubit A and B, coupled with coupling strength Ω have the same Hamiltonian. Figure 4.1 depicts the system. The spontaneous emission rate of qubit A and B are γ_A and γ_B respectively. The deliberate choice of unequal decay rates is motivated by the fact that EPs in this system emerge from the disparity between γ_A and γ_B [82]. As we will demonstrate later, increasing the difference between these decay rates leads to more pronounced effects on the system's entanglement dynamics.

Using interaction picture, the evolution of the system is described by the following quantum master equation [83]

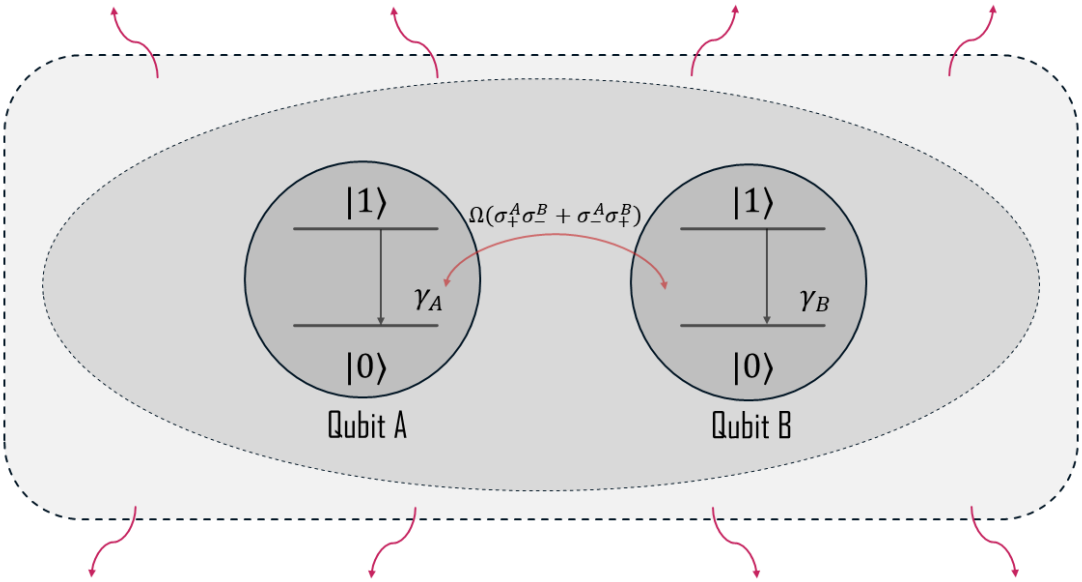

Figure 4.1: Two-qubit system

$$\frac{d\rho}{dt} = -i(H_{\text{eff}}\rho - \rho H_{\text{eff}}^{\dagger}) + \gamma_B \sigma_-^B \rho \sigma_+^B + \gamma_A \sigma_-^A \rho \sigma_+^A, \tag{4.1}$$

where

$$H_{\text{eff}} = \Omega(\sigma_+^A\sigma_-^B + \sigma_-^A\sigma_+^B) - \frac{1}{2}i\gamma_A\sigma_+^A\sigma_-^A - \frac{1}{2}i\gamma_B\sigma_+^B\sigma_-^B. \tag{4.2}$$

$\sigma_\pm^A$ and $\sigma_\pm^B$ are defined by

$$\sigma_\pm^B = I \otimes \sigma_\pm \tag{4.3}$$

and

$$\sigma_\pm^A = \sigma_\pm \otimes I, \tag{4.4}$$

where $\sigma_\pm = \frac{1}{2}(\sigma_1 \pm i\sigma_2)$, σ_i for $i = 1, 2, 3$ are the Pauli matrices. It can be shown that if we initiate the system as an X-state, where ρ_0 is given by

$$\rho_0 = \begin{pmatrix} a_0 & 0 & 0 & h_0^* \\ 0 & b_0 & m_0^* & 0 \\ 0 & m_0 & c_0 & 0 \\ h_0 & 0 & 0 & d_0 \end{pmatrix}, \tag{4.5}$$

then the system will evolve into an X-state as

$$\rho(t) = \begin{pmatrix} a(t) & 0 & 0 & h^*(t) \\ 0 & b(t) & m^*(t) & 0 \\ 0 & m(t) & c(t) & 0 \\ h(t) & 0 & 0 & d(t) \end{pmatrix}. \tag{4.6}$$

Therefore, we can vectorize the ρ into $\vec{\rho}$ as

$$\rho = \begin{pmatrix} a(t) & 0 & 0 & h^*(t) \\ 0 & b(t) & m^*(t) & 0 \\ 0 & m(t) & c(t) & 0 \\ h(t) & 0 & 0 & d(t) \end{pmatrix} \xrightarrow{\text{vectorization}} \vec{\rho} = \begin{pmatrix} a(t) \\ b(t) \\ c(t) \\ d(t) \\ m(t) \\ m^*(t) \\ h(t) \\ h^*(t) \end{pmatrix}. \tag{4.7}$$

Rewriting the master equation in terms of the Liouville operator, we have

$$\frac{d\vec{\rho}}{dt} = \mathcal{L}\vec{\rho}, \tag{4.8}$$

where $\mathcal{L}$ is

$$\mathcal{L} = \frac{1}{2} \begin{pmatrix} 0 & \gamma+\kappa & \gamma-\kappa & 0 & 0 & 0 & 0 & 0 \\ 0 & -\gamma-\kappa & 0 & \gamma-\kappa & -2i\Omega & 2i\Omega & 0 & 0 \\ 0 & 0 & -\gamma+\kappa & \gamma+\kappa & 2i\Omega & -2i\Omega & 0 & 0 \\ 0 & 0 & 0 & -2\gamma & 0 & 0 & 0 & 0 \\ 0 & -2i\Omega & 2i\Omega & 0 & -\gamma & 0 & 0 & 0 \\ 0 & 2i\Omega & -2i\Omega & 0 & 0 & -\gamma & 0 & 0 \\ 0 & 0 & 0 & 0 & 0 & 0 & -\gamma & 0 \\ 0 & 0 & 0 & 0 & 0 & 0 & 0 & -\gamma \end{pmatrix}. \tag{4.9}$$

The γ and κ are defined by

$$\gamma = \gamma_A + \gamma_B \tag{4.10}$$

and

$$\kappa = \gamma_B - \gamma_A. \tag{4.11}$$

Similar to the one-qubit case, we can simplify the analysis of the two-qubit system by reducing a variable while preserving its overall dynamics. In this thesis, we choose to normalize γ to the time scale by setting $\gamma = 1$. Normalizing Ω could also be beneficial since it naturally serves as a time scale for the dynamics, as discussed in Reference [84].

Additionally, we introduce a variable used by Han et al. [83] to facilitate the analysis of EPs, it is given by

$$\Omega = \frac{\kappa\eta}{4}. \tag{4.12}$$

4.3 Eigensystem

Similar to one-qubit, the dynamics of the system can be analyzed in terms of the eigenvalues and eigenvectors of Liouvillian superoperator $\mathcal{L}$. The eigenvalues of $\mathcal{L}$ are given by

$$\Lambda_1 = 0, \tag{4.13}$$
$$\Lambda_2 = -1, \tag{4.14}$$
$$\Lambda_3 = \Lambda_4 = \Lambda_5 = \Lambda_6 = -\frac{1}{2}, \tag{4.15}$$
$$\Lambda_7 = -\frac{1}{2} - \frac{1}{2}\kappa\sqrt{1-\eta^2}, \tag{4.16}$$
$$\Lambda_8 = -\frac{1}{2} + \frac{1}{2}\kappa\sqrt{1-\eta^2}. \tag{4.17}$$

The right eigenvectors are listed in Appendix C.1. For completeness, we will also work out the left eigenvectors. Mathematically, they must be biorthogonal to each other.

The structure of the eigensystem for two qubits are slightly different from one-qubit system. The system exhibits only third-order EP without exhibiting second-order EP. Third-order EP occurs when $\eta = \pm 1$, the system is underdamped when $|\eta| > 1$ and overdamped when $|\eta| < 1$, if we allow η to be negative.

At the EP, the generalized eigenvectors must be used to describe the system properly. When $\eta = \pm 1$, the left and right generalized eigenvectors are given by Appendix C.2.

4.4 Concurrence

Consider two qubits, labeled A and B, described by a density matrix ρ. The system is considered separable (not entangled) if ρ can be expressed as [76]

$$\rho = \sum_j w_j \rho_j^A \otimes \rho_j^B. \tag{4.18}$$

Since determining entanglement directly from this definition can be challenging, the degree of entanglement between the two qubits can be quantified using the concurrence C [25, 26], defined as

$$C = \max(0, \lambda_1 - \lambda_2 - \lambda_3 - \lambda_4), \tag{4.19}$$

where $\lambda_1, \lambda_2, \lambda_3, \lambda_4$ (with $\lambda_1 > \lambda_2 > \lambda_3 > \lambda_4$) are the eigenvalues of $\sqrt{\sqrt{\rho}\tilde{\rho}\sqrt{\rho}}$ arranged in descending order, and $\tilde{\rho}$ is defined by

$$\tilde{\rho} = (\sigma_2 \otimes \sigma_2)\rho^*(\sigma_2 \otimes \sigma_2). \tag{4.20}$$

The calculation of concurrence simplifies significantly for the X-state as shown in equation (4.6). The concurrence for this state is computed as

$$C = \max(0, C_1, C_2), \tag{4.21}$$

where

$$C_1 = 2(|m| - \sqrt{ad}), \tag{4.22}$$

$$C_2 = 2(|h| - \sqrt{bc}). \tag{4.23}$$

The concurrence ranges from 0, indicating a non-entangled state, to 1, denoting a maximally entangled state. For this analysis, we consider specific initial conditions that mix maximally entangled, $|\Phi(\theta)\rangle$ and $|\Psi(\theta)\rangle$, and maximally mixed states, $I/4$, convexly,

$$\rho_\Psi(\theta, p) = p\,|\Psi(\theta)\rangle\langle\Psi(\theta)| + (1-p)\frac{I}{4}, \tag{4.24}$$

$$\rho_\Phi(\theta, p) = p\,|\Phi(\theta)\rangle\langle\Phi(\theta)| + (1-p)\frac{I}{4}. \tag{4.25}$$

The maximally entangled states, $|\Psi(\theta)\rangle$ and $|\Phi(\theta)\rangle$ [75, 79], are defined as

$$|\Phi(\theta)\rangle = (U(\theta) \otimes I)\,|\Phi_+\rangle\,, \tag{4.26}$$

$$|\Psi(\theta)\rangle = (U(\theta) \otimes I)\,|\Psi_+\rangle\,, \tag{4.27}$$

where

$$|\Phi_+\rangle = \frac{1}{\sqrt{2}}(|00\rangle + |11\rangle), \tag{4.28}$$

$$|\Psi_+\rangle = \frac{1}{\sqrt{2}}(|01\rangle + |10\rangle). \tag{4.29}$$

Here, U is a unitary transformation applied on first qubit, defined as

$$U(\theta) = \begin{pmatrix} 1 & 0 \\ 0 & e^{i\theta} \end{pmatrix}. \tag{4.30}$$

We will call θ as phase angle, which takes values in the range 0 to 2π. The study by Du et al. [79] demonstrates that states of the form given in equations (4.26) and (4.27) can be experimentally observed. Furthermore, combining this with the study by Liu et al. [80] and Jiang et al. [81], which shows that the Werner state can be experimentally prepared, suggests that states of the form of equations (4.24) and (4.25) can also be realized in the laboratory.

Next, we determine the eigenvalues of both $\rho_\Psi(\theta, p)$ and $\rho_\Phi(\theta, p)$. Notably, these matrices share the same eigenvalues, which are given by $(1-p)/4$ and $(1+3p)/4$. Since the properties of a density matrix require its eigenvalues to be non-negative, this imposes the constraint $-1/3 < p \leq 1$. Within this range, the interval $-1/3 < p \leq 1/3$ corresponds to a separable (not entangled) state, while $1/3 < p \leq 1$ corresponds to an entangled state. In this study, we focus on two extreme cases, $p = 1/3$, which represents a separable state, and $p = 1$, which corresponds to a maximally entangled state.

Chapter 5

Analysis on two-qubit

We need to investigate how the phase angle θ of the initial state would affect the evolution from $\theta = 0$ to $\theta = 2\pi$ at a step of $\pi/2$. Numerically, we can show that the maximum concurrence always occurs at $\kappa = \pm 1$ if we start the system disentangled as shown in Figure 5.1. Since a system with negative κ is equivalent to one with positive κ and negative η shown in equation (4.12), we will adopt the latter convention for our research. Mathematically, the structure of concurrence consists of the terms $\cosh\left(\sqrt{1-\eta^2}\kappa t/2\right)$ and $\sinh\left(\sqrt{1-\eta^2}\kappa t/2\right)$. For overdamping where $|\eta| < 1$, larger κ causes the terms to blow up faster. Therefore, the concurrence reaches higher maximum compared to concurrence with smaller κ. For underdamping where $|\eta| > 1$, higher κ implies higher frequency of oscillation. Therefore, reaching the maxima of the concurrence requires lesser time than concurrence with smaller κ. Since reaching maximum requires lesser time, the decay of higher κ system will not be severed compared to smaller κ at initial stage of evolution. We will use $\kappa = 1$ as our parameter for the rest of the research.

5.1 Initial state: $\rho_\Psi(\theta, p)$ for $p = 1/3$ and $p = 1$

We start with the initial state of $\rho_\Psi(\theta, 1/3) = |\Psi(\theta)\rangle\langle\Psi(\theta)|/3 + I/6$ where the initial concurrence is $C(0) = 0$. When $\theta = 0$, we have the contour graph of concurrence, C vs t and η shown in Figure 5.2(a). We can see that the structure of concurrence is symmetrical with respect to $\eta = 0$. The maximum concurrence occur when $\eta = \pm 0.94$, which is approximately 0.06 away from nearest third-order EP of the system. The entanglement generation stopped when $|\eta| > 4.45$.

When the $\theta = \pi/2$, we have the contour graph of concurrence, C vs t and η shown in Figure 5.2(b). The symmetrical properties of the contour graph is broken, the entanglement generations are more likely when $\eta < 0$. The maximum concurrence occur when $\eta = -1.31$, which is approximately 0.31 away from third-order EP $\eta = -1$. The entanglement generation stopped when $\eta > 2.05$. For $\theta = \pi$, the contour graph returned to the structure of $\theta = 0$. For $\theta = 3\pi/2$, the

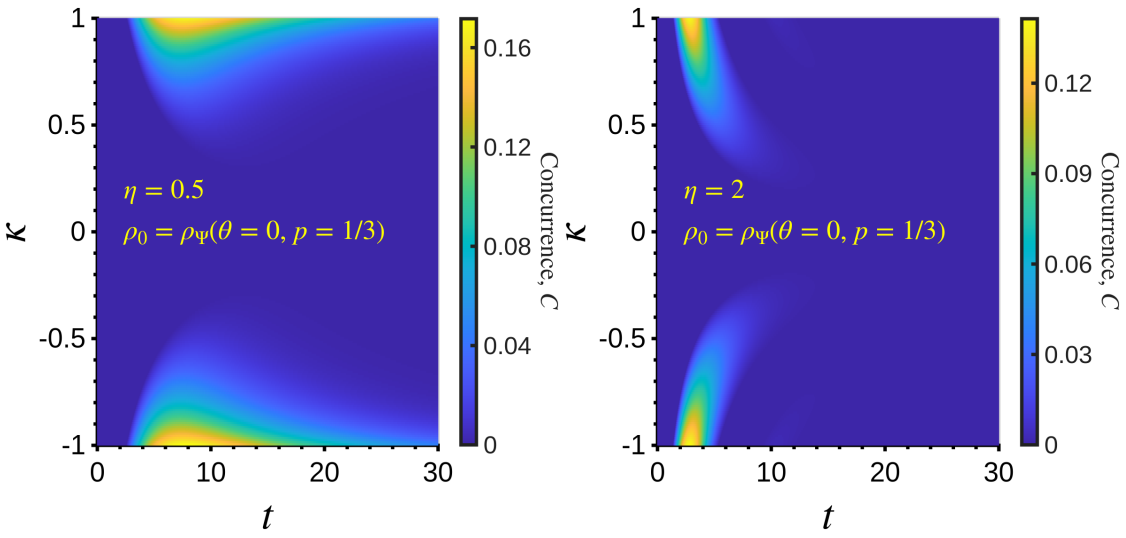

(a) (b)

Figure 5.1: Contour graphs of concurrence, C vs t and κ for initial state of $\rho_\Psi(\theta = 0, p = 1/3)$. (a) Graph for $\eta = 0.5$. (b) Graph for $\eta = 2$.

structure of contour graph is the same as the reflection of $\theta = \pi/2$ on $\eta = 0$.

Theoretically, the concurrence of the system will evolve under the $C_1(t)$ given in equation (4.22). The reason is that the initial state of $h_0 = 0$ implies $h(t) = 0$, causing $C_2(t)$ to be always negative. This can be seen by considering the element $h(t)$ from equations (4.8) and (4.9), we arrive to following first order differential equation

$$\frac{d}{dt}h(t) = -\frac{\lambda}{2}h(t). \tag{5.1}$$

Thus, $h_0 = 0$ implies $h(t) = 0$ from equation (5.1). On the other hand, the terms of $C_1(t)$, which are $|m|$ and $\sqrt{ad}$, will affects the state of entanglement of the system, where $m(t), a(t)$ and $d(t)$ can be solved readily and are given by

$$\begin{aligned} a(t) =& -\frac{\eta(3\eta + \sin(\theta)) - (\eta\sin(\theta) + 3)\cosh\left(\frac{1}{2}\sqrt{1-\eta^2}\kappa t\right)}{3(\eta^2 - 1)}e^{-\frac{t}{2}} \\ &+ d(t) + 1, \end{aligned} \tag{5.2}$$

$$d(t) = \frac{1}{6}e^{-t}, \tag{5.3}$$

$$\begin{aligned} m(t) =& -\frac{-3\eta + \sin(\theta) + \eta(-\eta\sin(\theta) + 3)\cosh\left(\frac{1}{2}\sqrt{1-\eta^2}\kappa t\right)}{6(\eta^2 - 1)}ie^{-\frac{t}{2}} \\ &+ \frac{1}{6}e^{-\frac{t}{2}}\cos(\theta), \end{aligned} \tag{5.4}$$

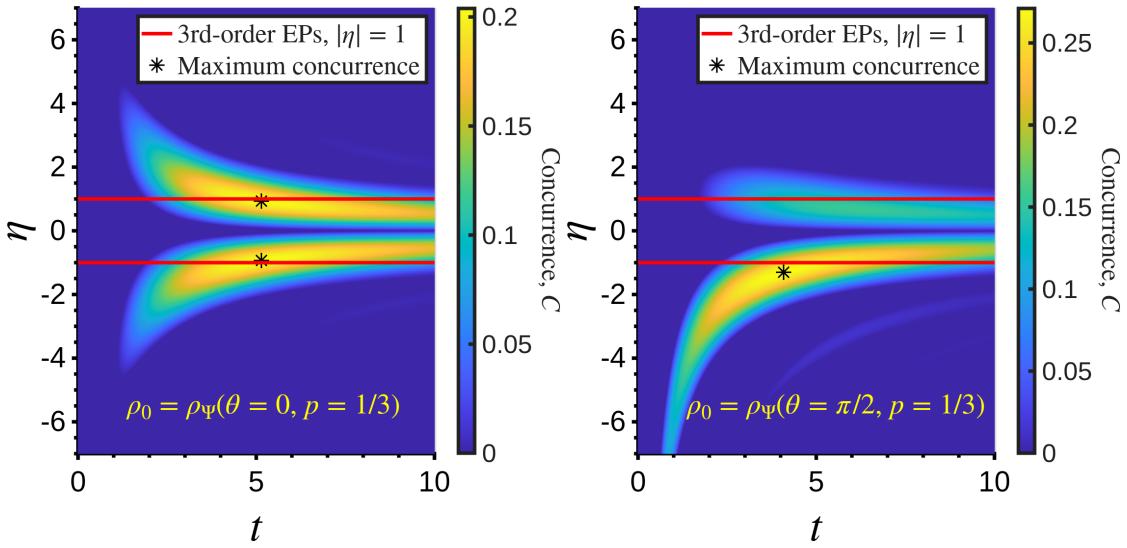

Figure 5.2: Contour graphs of concurrence, C vs t and η for initial state of $\rho_\Psi(\theta, p = 1/3)$. The red lines indicates $|\eta| = 1$, the EPs. (a) Graph for $\theta = 0$ and $\theta = \pi$, maximum concurrence occurred at $|\eta| = 0.94$ away from EPs. (b) Graph for $\theta = \pi/2$, maximum concurrence occurred at $\eta = -1.31$ away from EP. The graph of $\theta = 3\pi/2$ is the reflection of the graph for $\theta = \pi/2$ with respect to $\eta = 0$.

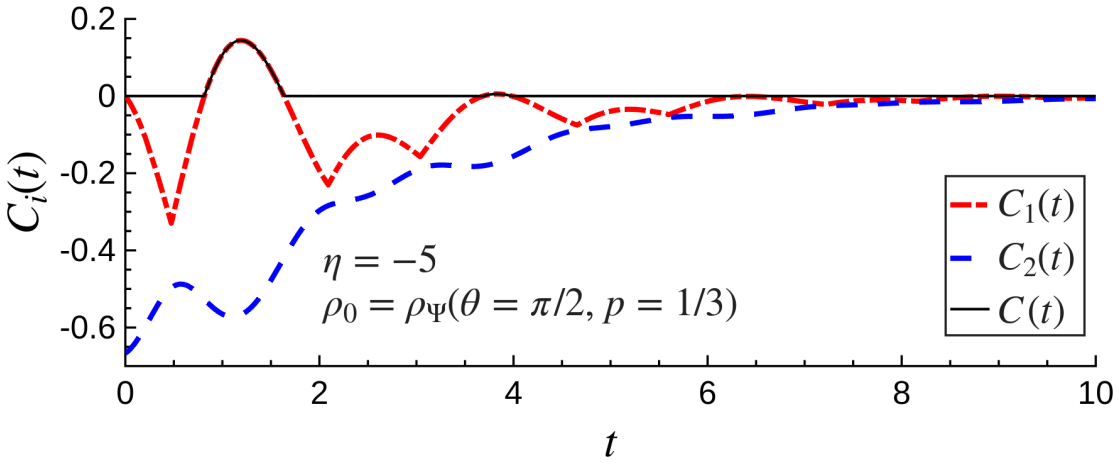

Figure 5.3: Graph of Concurrence, C vs t for initial state of $\rho_\Psi(\theta = \pi/2, p = 1/3)$, where $\eta = -5$.

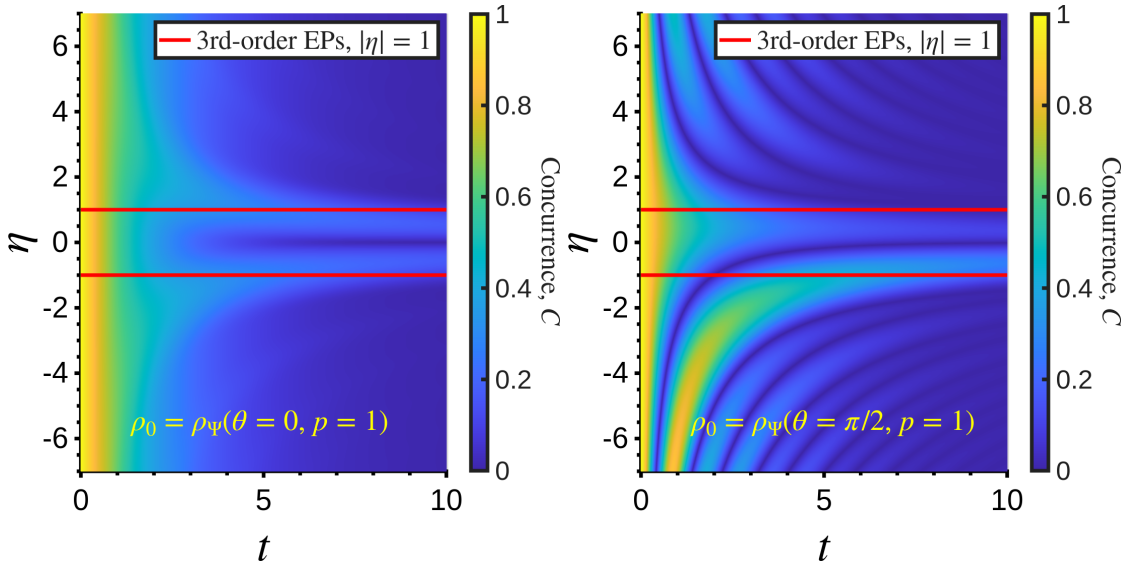

Figure 5.4: Contour graphs of concurrence, C vs t and η for initial state of $\rho_\Psi(\theta, p = 1)$ with rotating variable of (a) $\theta = 0, \pi$, (b) $\theta = \pi/2$. The red lines indicates $|\eta| = 1$, the EPs. The graph of $\theta = 3\pi/2$ is the reflection of graph of $\theta = \pi/2$ with respect to $\eta = 0$.

and the concurrence $C(t)$ is given by

$$C(t) = C_1(t) = |m(t)| - \sqrt{a(t)d(t)} \tag{5.5}$$

The system is entangled when $|m| > \sqrt{ad}$ and untangled when $|m| \leq \sqrt{ad}$.

From $C(t)$, we can see that for $|\eta| < 1$, which is overdamping, the concurrence is governed by the decaying terms on $\sinh\left(t\sqrt{1-\eta^2}/2\right)$ and $\cosh\left(t\sqrt{1-\eta^2}/2\right)$. When $|\eta| > 1$, the concurrence is governed by the oscillating terms $\sin\left(t\sqrt{\eta^2-1}/2\right)$ and $\cos\left(t\sqrt{\eta^2-1}/2\right)$. However, the oscillating feature is not apparent according to Figure 5.2. This can be explained by Figure 5.3 which shows $C_1(t)$ and $C_2(t)$ function for $\theta = \pi/2$ at $\eta = -5$, where the oscillatory feature of $C_1(t)$ is most of the time negative, hence does not contribute to concurrence.

We now investigate the system with the initial state of $\rho_\Psi\ (\theta, p = 1) = |\Psi(\theta)\rangle\langle\Psi(\theta)|$ where the initial concurrence is $C(0) = 1$. When the $\theta = 0$, we have the contour graph of concurrence, C vs t and η shown in Figure 5.4(a). We can see that the structure of concurrence is symmetrical with respect to $\eta = 0$. The oscillating feature in underdamping region is not apparent for $\theta = 0$.

We can see that the concurrence start to have oscillating behavior when $\theta = \pi/2$ in the underdamped region, $|\eta| > 1$, shown in Figure 5.4(b). The symmetry of the contour graph is broken for opposite sign of η. The second maxima for $\eta < 0$ is much larger than $\eta > 0$ as shown in Figure 5.5(b). When $\theta = \pi/2$, for $\eta > 0$ in

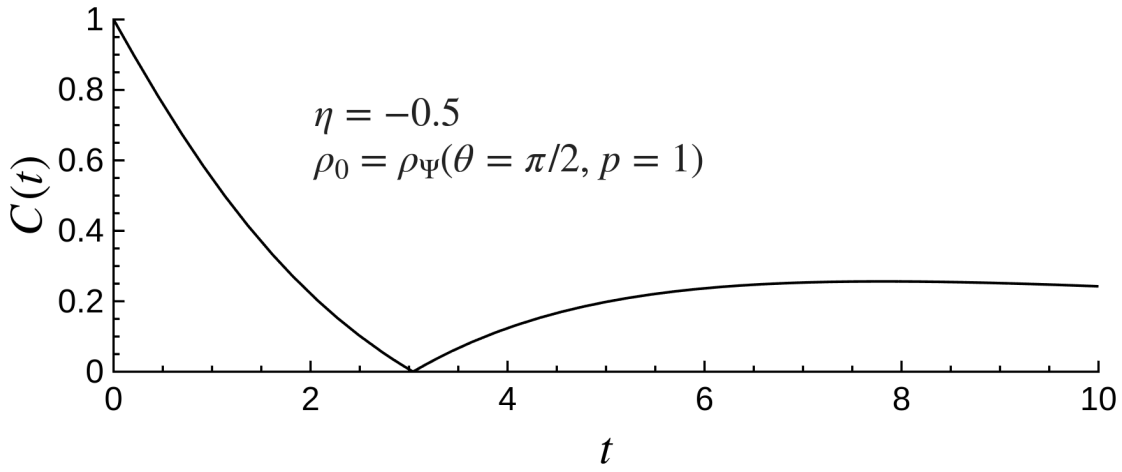

(a)

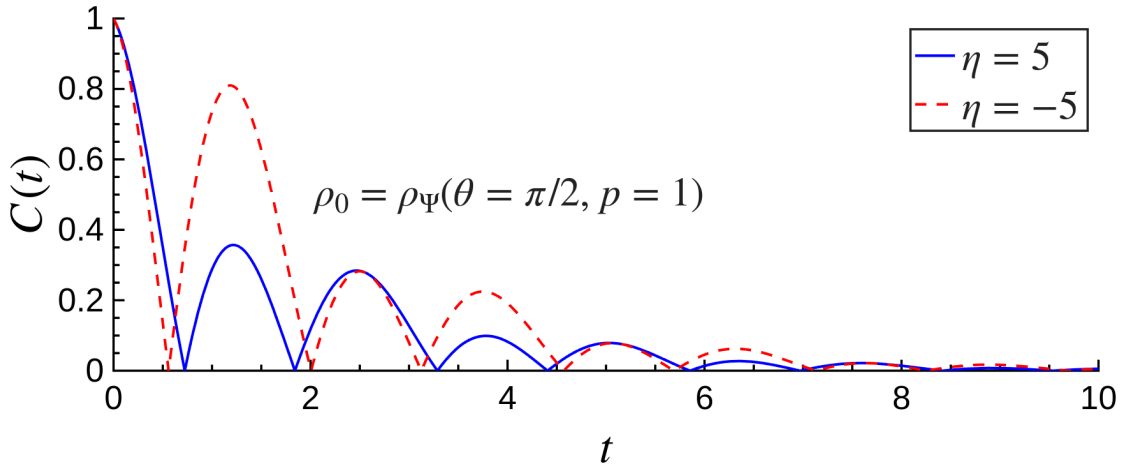

(b)

Figure 5.5: Graph of concurrence, C vs t for initial state of $\rho_\Psi(\theta = \pi/2, p = 1)$, where (a) $\eta = -0.5$ showing ESD immediately followed by entanglement generation and (b) $\eta = \pm 5$ showing second maxima for $\eta = -5$ is much larger than $\eta = 5$.

overdamped region, the concurrence decay slowly into zero, without any second entanglement generation. For $-1 < \eta < 0$ in overdamped region, there will be an entanglement sudden death and followed by immediate entanglement generation shown in Figure 5.5(a). For $\theta = \pi$, the contour graph returned to the structure of $\theta = 0$. For $\theta = 3\pi/2$, the structure of contour graph is the same as the reflection of $\theta = \pi/2$ on $\eta = 0$.

Next, we investigate the analytic solution of concurrence for the system with initial state of $\rho_\Psi(\theta, p = 1) = |\Psi(\theta)\rangle\langle\Psi(\theta)|$. The concurrence of the system is also given by $C_1(t)$, which is similar to previous cases, because of $h(t) = 0$. The $C_1(t)$ can be separated into two parts, $|m|$ and $\sqrt{ad}$. However, the element $\sqrt{ad}$ is zero since the element $d(t)$ of the system is always zero. Therefore, the concurrence only depends on the magnitude of complex function $m(t)$, given by

$$m(t) = -\frac{-\eta - p\sin(\theta) + \eta(\eta p \sin(\theta) + 1)\cosh\left(\frac{1}{2}\sqrt{1-\eta^2}\kappa t\right)}{2(\eta^2 - 1)} i e^{-\frac{t}{2}} + \frac{1}{2} p e^{-\frac{t}{2}} \cos(\theta). \tag{5.6}$$

The concurrence of the system is then given by

$$C(t) = \left| \frac{\eta \cosh\left(\frac{1}{2}\sqrt{1-\eta^2}\kappa t\right) + 1}{\eta + 1} \right| e^{-\frac{t}{2}} \tag{5.7}$$

and

$$C(t) = \left| \frac{\eta \cosh\left(\frac{1}{2}\sqrt{1-\eta^2}\kappa t\right) - 1}{\eta - 1} \right| e^{-\frac{t}{2}}, \tag{5.8}$$

for $\theta = \pi/2$ and $\theta = 3\pi/2$ respectively. For $\theta = 0$ and $\theta = \pi$, the concurrence is given by

$$C(t) = \sqrt{1 + \frac{4\eta^2 \sinh^4\left(\frac{1}{4}\sqrt{1-\eta^2}\kappa t\right)}{(\eta^2 - 1)^2}} e^{-\frac{t}{2}}. \tag{5.9}$$

5.2 Initial state: $\rho_\Phi(\theta, p)$ for $p = 1/3$ and $p = 1$

We start the system with initial state $\rho_\Phi(\theta, p = 1/3) = |\Phi(\theta)\rangle\langle\Phi(\theta)|/3 + I/6$, where initial concurrence is $C(0) = 0$. As we can see from Figure 5.6(a), the structure of concurrence is symmetrical with respect to $\eta = 0$. The symmetrical property of concurrence's structure can be deduced directly from exact equation of concurrence given by

$$C(t) = C_1(t) = \frac{2|\eta| \sinh^2(\frac{1}{4}\sqrt{1-\eta^2}\kappa t)}{|\eta^2 - 1|} e^{-\frac{t}{2}} - 2\sqrt{a(t)d(t)}, \tag{5.10}$$

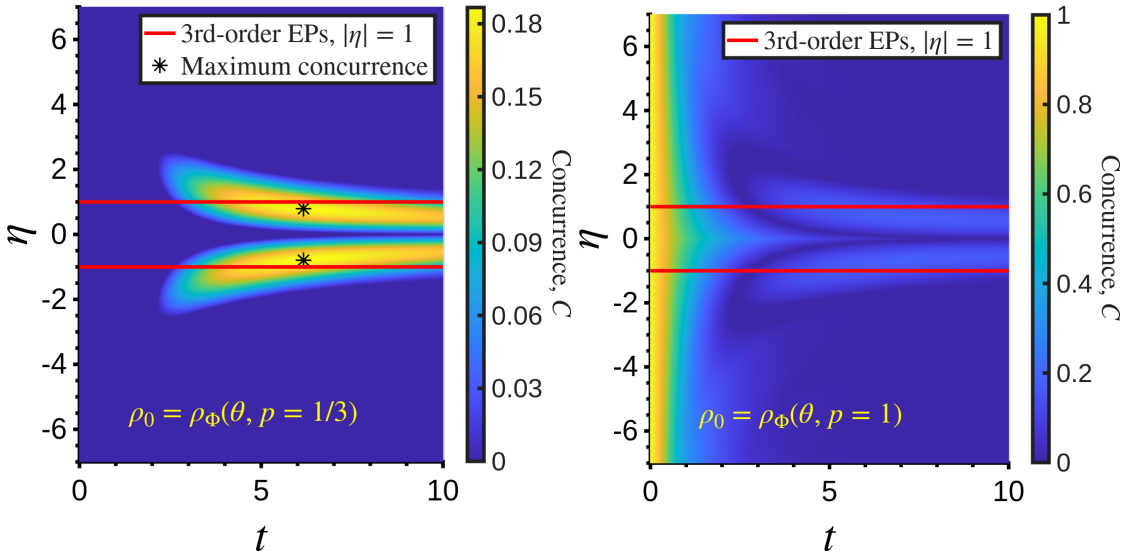

Figure 5.6: Contour graphs of concurrence, C vs t and η. The red lines indicates $|\eta| = 1$, the EPs. Graph (a) represents initial state $\rho_\Phi(\theta, p = 1/3)$, where maximum concurrence occur at $|\eta| = 0.8$ away from EPs and (b) represents initial state $\rho_\Phi(\theta, p = 1)$ for $0 \leq \theta \leq 2\pi$.

where

$$a(t) = -\frac{\eta^2 - \cosh\left(\frac{1}{2}\sqrt{1-\eta^2}\kappa t\right)}{\eta^2 - 1} e^{-\frac{t}{2}} + d(t) + 1, \tag{5.11}$$

$$d(t) = \frac{1}{3} e^{-t}. \tag{5.12}$$

The maximum concurrence occur when $|\eta| = 0.80$, which is approximately 0.20 away from third-order EPs $|\eta| = 1$. The entanglement generation stopped when $|\eta| > 2.52$. Another surprising properties for this system is that the structure of the concurrence is independent to the phase angle θ, which is in contrary to the system with initial state of $\rho_\Psi(\theta, p = 1/3)$. The phase angle of the system is also reflected in the equation of concurrence given by equation (5.10).

Theoretically, the phase invariance of concurrence can be understood by considering each element of X-state. For the system with initial state of $\rho_\Phi(\theta, p = 1/3)$, the only element that depends on variable θ is

$$h(t) = \frac{1}{6} e^{-\frac{1}{2} - i\theta}. \tag{5.13}$$

However, the magnitude, $|h(t)|$ does not depends on θ implying that the concurrence of the system does not depends on θ. For this system, the concurrence only depends on $C_1(t)$, given by equation (5.10), which is responsible for entanglement generation.

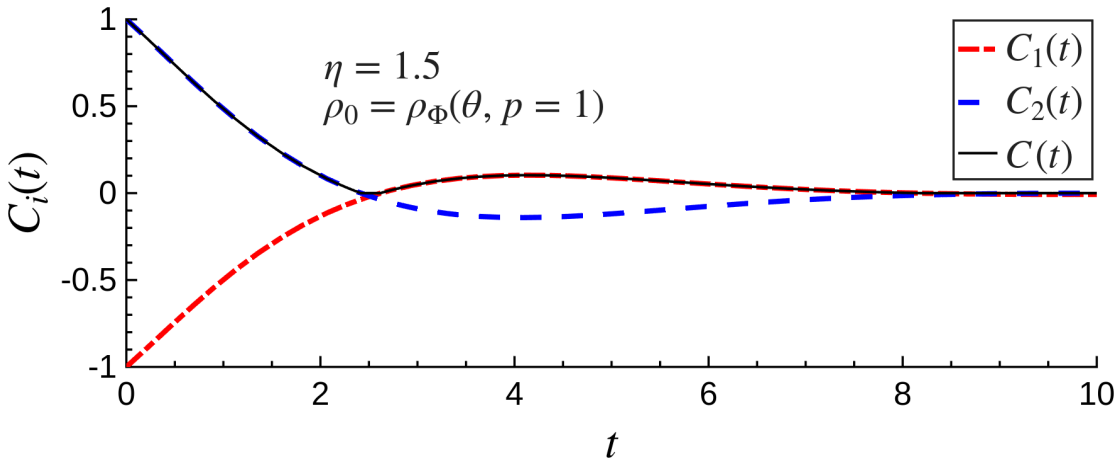

(a)

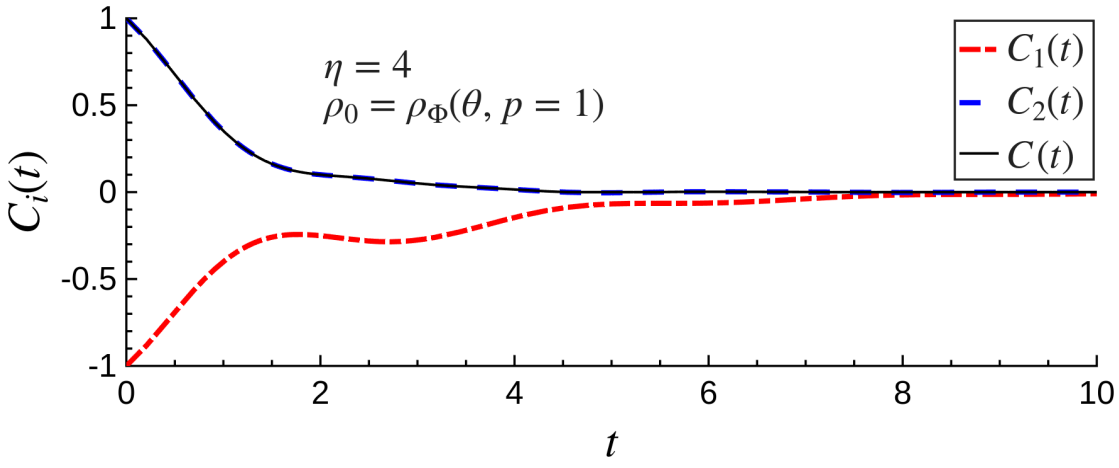

(b)

Figure 5.7: Graph of concurrence, C_1, C_2 vs t for initial state of $\rho_\Phi(\theta, p = 1)$ where (a) $\eta = 1.5$ showing ESD immediately followed by entanglement generation and (b) $\eta = 4$ showing ESD only.

Next, we investigate the system with initial state of $\rho_\Phi(\theta, p = 1) = |\Phi(\theta)\rangle\langle\Phi(\theta)|$ where the initial concurrence is $C(0) = 1$. As we can see from Figure 5.6(b), the structure of concurrence is symmetrical with respect to $\eta = 0$. This property is reflected by the following concurrence function of this system $C(t) = \max(0, C_1(t), C_2(t))$ given by equation (4.21) where

$$C_1(t) = \frac{2|\eta| \sinh^2(\frac{1}{4}\sqrt{1-\eta^2}\kappa t)}{|\eta^2 - 1|} e^{-\frac{t}{2}} - 2\sqrt{a(t)d(t)}, \tag{5.14}$$

$$C_2(t) = e^{-\frac{t}{2}} - \sqrt{(a(t) + d(t) - 1)^2 + \frac{\sinh^2(\frac{1}{2}\sqrt{1-\eta^2}\kappa t)}{\eta^2 - 1} e^{-t}}, \tag{5.15}$$

and

$$a(t) = -\frac{\eta^2 - \cosh\left(\frac{1}{2}\sqrt{1-\eta^2}\kappa t\right)}{\eta^2 - 1} e^{-\frac{t}{2}} + d(t) + 1, \tag{5.16}$$

$$d(t) = \frac{1}{2} e^{-t}. \tag{5.17}$$

Similar to previous system where initial state is $\rho_\Phi(\theta, p = 1/3)$, this system is also phase invariance, reflected by equations (5.14) and (5.15). We can see from Figure 5.6(b), the sudden death followed by immediate entanglement generation occur in the range of $|\eta| < 2.08$, reflected by Figure 5.7(a).

Similarly, the phase invariance of concurrence is because the only element that depends on variable θ is

$$h(t) = \frac{1}{2} e^{-\frac{1}{2} - i\theta}. \tag{5.18}$$

However, the magnitude, $|h(t)|$ does not depends on θ implying that the concurrence of the system does not depends on θ. For this system, the concurrence depends on both $C_1(t)$ and $C_2(t)$ for $|\eta| < 2.08$. The concurrence before sudden death is governed by $C_2(t)$ given in equation (5.14) and followed by immediate entanglement generation which is governed by $C_1(t)$ given in equation (5.15) which can be seen by Figure 5.7(a). For concurrence outside of $|\eta| < 2.08$, the system only undergoes sudden death shown in Figure 5.7(b). Therefore, the concurrence depends only on $C_2(t)$.

5.3 Discussion

We begin by discussing the role of EPs in the system. A clear transition in entanglement dynamics from an overdamped to an underdamped regime across the EPs can be distinctly observed when the system is initialized in the pure state $\rho_\psi(\theta = \pi/2, p = 1)$ shown in Figure 5.4(b). For other initial states, this transition is less apparent. This is because either the amplitude of oscillations is significantly

suppressed, or the oscillatory behavior manifests in regions where the concurrence components C_1 and C_2 are negative, as illustrated in Figure 5.3. These findings support the interpretation of EPs as boundaries of dynamical phase transitions [7, 38].

Furthermore, the emergence of EPs is fundamentally linked to the disparity between the decay rates γ_A and γ_B [82]. Physically, this imbalance breaks the symmetry between the two qubits, and when combined with coupling, it gives rise to the exotic dynamics characteristic of EPs.

Next, we turn to the role of the phase angle θ. The concurrence of the initial state, $\rho_\Psi(\theta, p)$, depends on the phase angle θ, where it has not been explicitly addressed in prior research. This feature is significant because experimentally prepared states [79], such as $\rho_\Psi(\theta, p)$, may be influenced by their intrinsic phase angle, leading to different outcomes despite appearing to be identical.

In the context of quantum computing, this dependency is particularly important. The amplitude of concurrence oscillations can be adjusted through the phase angle of the initial state $\rho_\Psi(\theta, p = 1)$ (cf. Figure 5.4), allowing for control over the desired quantum computing outcomes.

For $\rho_\Psi(\theta, p = 1/3)$ (cf. Figure 5.2), EPs serve as a rough approximation for achieving higher concurrence. However, the maximum concurrence often occurs away from EPs, $|\eta| = 1$, specifically at $\eta = \pm 0.94$ for $\theta = 0, \pi$ and $\eta = -1.31, 1.31$ for $\theta = \pi/2, 3\pi/2$ respectively. Despite the maximum concurrence does not align precisely with the system's EPs, the EPs still provide a useful guideline for generating more entangled two-qubit states, benefiting quantum computing processes. Furthermore, by tuning the phase angle, the maximum concurrence can be shifted towards either the positive or negative part of η, enhancing the overall concurrence and providing greater flexibility in quantum state preparation for specific applications.

The concurrence of the initial state $\rho_\Phi(\theta, p)$ is phase invariance (cf. Figure 5.6), which is significant for the stability of quantum computing applications. This independence ensures that the same results can be achieved without the need to account for variations in the phase angle of $\rho_\Phi(\theta, p)$. The downside of phase invariance is that it provides limited tunability compared to the state that depends on phase angle.

For the initial state $\rho_\Phi(\theta, p = 1/3)$ (cf. Figure 5.6(a)), the maximum concurrence occurs at $|\eta| = 0.80$ for all θ, which is away from EPs $|\eta| = 1$. Similar to the case of $\rho_\Psi(\theta, p = 1/3)$ (cf. Figure 5.6(b)), EPs still provide a useful guideline for generating more entangled two-qubit states. However, the key differences lie in the symmetrical nature of the concurrence with respect to the sign of η for $\rho_\Phi(\theta, p = 1/3)$ and its independence from the phase angle. As a result, the maximum concurrence cannot be further increased by varying the phase angle, unlike $\rho_\Psi(\theta, p = 1/3)$.

Up to this point, it might seem that if we initiate the state with zero concurrence, $C(0) = 0$, the maximum concurrence will occur around EPs. However,

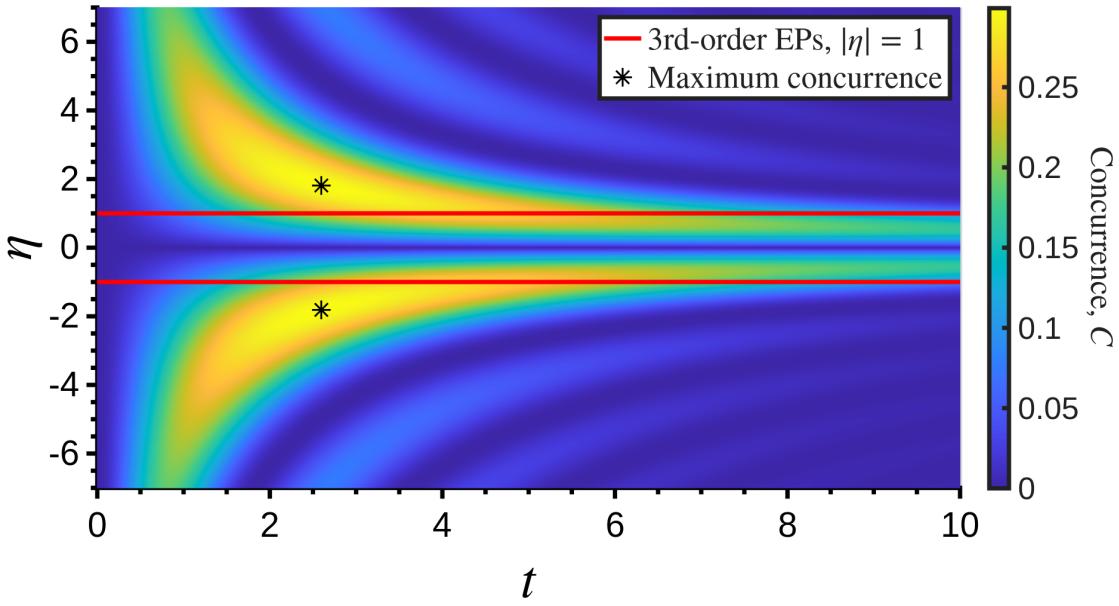

Figure 5.8: Contour graphs of concurrence, C vs t and η for initial state of $\rho(0) = 1/2(|10\rangle\langle 10| + |01\rangle\langle 01|)$. The red lines indicates $|\eta| = 1$, the EPs. Maximum concurrence occur around $|\eta| = 1.82$

this is not universally true. Figure 5.8 shows contour graph of concurrence for initial state of $\rho(0) = 1/2(|10\rangle\langle 10| + |01\rangle\langle 01|)$, the maximum concurrence occur at $|\eta| = 1.82$. These values are significantly farther from the EPs at $|\eta| = 1$ compared to the systems with initial states of $\rho_\Psi(\theta, p = 1/3)$ and $\rho_\Phi(\theta, p = 1/3)$. This highlights the crucial role of the initial state in shaping the entanglement dynamics, as also emphasized in Reference [82].

5.4 Markovian limit

Everything discussed so far has been derived under the Markovian approximation in the study of open quantum systems. This assumption is generally valid when the interaction between the system and its environment is weak and memoryless [3]. However, this poses limitations when attempting to describe more realistic physical systems, where stronger coupling or memory effects cannot be neglected. This raises new questions: Will the phase angle applied to the initial quantum state exhibit novel or exotic features in entanglement dynamics beyond the Markovian regime? Will the role and position of EPs persist, shift, or even vanish when non-Markovian dynamics are considered?

Several studies have recently begun to address these questions, particularly regarding EPs. For instance, EPs have been shown to exist within non-Markovian open quantum systems, with experimental evidence obtained by tuning a measurable quantity called the effective decay rate of a qubit [85]. The same work

highlights a compelling interplay between non-Markovianity, the Quantum Zeno effect, and non-Hermitian dynamics. On the computational side, recent advances have enabled the exploration of EPs in non-Markovian systems using exact numerical methods, such as the pseudomode equation of motion (PMEOM) and hierarchical equations of motion (HEOM) [86].

These developments point to a promising and largely untapped research frontier. While this thesis has focused on the Markovian regime, future investigations could extend the analysis to non-Markovian systems to uncover richer entanglement behavior and potentially novel forms of EPs. This direction may not only clarify the robustness of phase control in realistic environments but also inform experimental designs for quantum information protocols under strong system-environment coupling.

Chapter 6

Conclusion

6.1 Summary of findings

This thesis investigated the dynamics of one- and two-qubit systems in open quantum environment, focusing on the role of EPs on the entanglement dynamics. The study addressed critical questions about how EPs affect two-qubit system dynamics, and the impact of phase changes in the initial state on entanglement structure.

The research began by introducing the dynamics of a one-qubit open quantum system using the GKSL equation. The concept of EPs was explored through changes in eigenvalues and eigenvectors, with generalized eigenvectors derived for second- and third-order EPs to capture system behavior at these points. A parameter space diagram was constructed to visualize EP occurrence and its connection to overdamped, underdamped and critically damped region.

The study was then extended to a coupled two-qubit system, incorporating phase angle in the initial state. We deliberately normalize γ by setting $\gamma = 1$ and choose $\kappa = 1$ to maximize the effect on concurrence. The initial states represented by $\rho_\Psi(\theta, p)$ demonstrated entanglement dynamics dependent on phase angle. For $\rho_\Psi(\theta, p = 1)$, the amplitude of oscillating concurrence was maximal at $\theta = \pi/2$ and $\theta = 3\pi/2$, and minimal at $\theta = 0$ and $\theta = \pi$.

In contrast, for $\rho_\Psi(\theta, p = 1/3)$, the oscillatory behavior was significantly reduced. In this case, the maximum concurrence occurrs at $\eta = \pm 0.94$, away from EPs, $|\eta| = 1$, when $\theta = 0$. As the phase angle θ deviated from 0, the symmetric structure of concurrence breaks, causing the maximum concurrence to shift and increase towards the negative part of η. Similarly, when θ increases beyond π, the maximum concurrence shifts and increases towards positive part of η.

For the initial state $\rho_\Phi(\theta, p)$, the concurrence exhibits phase invariance and retains a symmetric structure around $\eta = 0$. For $\rho_\Phi(\theta, p = 1/3)$, the maximum concurrence is also observed at $\eta = \pm 0.80$, away from the EPs at $|\eta| = 1$. However, for $\rho_\Phi(\theta, p = 1)$, the concurrence features entanglement sudden death (ESD) followed by immediate entanglement regeneration within the region $|\eta| < 2.08$.

6.2 Future research directions

Building on these findings, several avenues for future research emerge. First, experimental validation of the theoretical models developed in this thesis is crucial. Such experimental studies would not only confirm the theoretical insights but also provide a more nuanced understanding of the role of EPs and phase angle in quantum dynamics.

Secondly, an exploration of the impact of environmental factors, such as noise and thermal fluctuations, on the stability of entanglement near EPs, could yield valuable insights for the development of resilient quantum technologies. Additionally, further investigation into the influence of phase angle and EP on entanglement dynamics, especially in multi-qubit systems, may reveal new strategies for optimizing quantum computing application. Extending this line of inquiry to non-Markovian systems, which are characterized by memory effects, could also enhance our understanding of long-term entanglement behavior.

Finally, applying these findings to emerging quantum technologies, such as quantum sensors, quantum communication, and quantum information, represents a crucial step towards bridging the gap between theoretical research and practical applications. By addressing these avenues, future research can build on the foundational work of this thesis, driving advancements in quantum mechanics and its technological applications.

Part III

Appendixes

Appendix A

Generalized eigenvectors for one-qubit

A.1 Second-order exceptional points

For second-order EP, two eigenvalues and eigenvectors coalesce. One more generalized eigenvector is needed to complete the eigenspace. The right generalized eigenvectors, $\vec{v}_1, \vec{v}_2, \vec{v}_3, \vec{v}_4$ can be solved by following eigenvector equation and Jordan chain.

$$(\mathcal{L} - \Lambda_1 I)\vec{v}_1 = 0, \tag{A.1}$$
$$(\mathcal{L} - \Lambda_2 I)\vec{v}_2 = 0, \tag{A.2}$$
$$(\mathcal{L} - \Lambda_3 I)\vec{v}_3 = 0, \tag{A.3}$$
$$(\mathcal{L} - \Lambda_3 I)\vec{v}_4 = \vec{v}_3, \tag{A.4}$$

where the eigenvalues are given by equations (3.10) to (3.11). Solving the right generalized eigenvector, we have

$$\vec{v}_1 = \frac{1}{8d^2 + 4\delta^2 + 1} \begin{pmatrix} 4d^2 + 4\delta^2 + 1 \\ 4d^2 \\ -2d(2\delta + i) \\ -2d(2\delta - i) \end{pmatrix}, \tag{A.5}$$

$$\vec{v}_2 = N_2 \begin{pmatrix} 2d(2\Lambda_2 + 1) \\ -2d(2\Lambda_2 + 1) \\ (\Lambda_2 + 1)(2\delta + i(2\Lambda_2 + 1)) \\ (\Lambda_2 + 1)(2\delta - i(2\Lambda_2 + 1)) \end{pmatrix}, \tag{A.6}$$

$$\vec{v}_3 = N_3 \begin{pmatrix} 2d(2\Lambda_3 + 1) \\ -2d(2\Lambda_3 + 1) \\ (\Lambda_3 + 1)(2\delta + i(2\Lambda_3 + 1)) \\ (\Lambda_3 + 1)(2\delta - i(2\Lambda_3 + 1)) \end{pmatrix}, \tag{A.7}$$

$$\vec{v}_4 = -\frac{N_3}{1+2\Lambda_3}\begin{pmatrix} 0 \\ 0 \\ 2\delta - i(2\Lambda_3+1)^2 \\ 2\delta + i(2\Lambda_3+1)^2 \end{pmatrix}, \tag{A.8}$$

where

$$N_2 = \frac{1}{4d\Lambda_2((2\Lambda_2+1)^2(4\Lambda_2+3) - 4\delta^2)}, \tag{A.9}$$

$$N_3 = \frac{2\Lambda_3+1}{8d\Lambda_3(4\delta^2 + (2\Lambda_3+1)^3)}. \tag{A.10}$$

The left generalized eigenvectors can be solved by following

$$(\mathcal{L}^\dagger - \Lambda_1^* I)\vec{u}_1 = 0, \tag{A.11}$$

$$(\mathcal{L}^\dagger - \Lambda_2^* I)\vec{u}_2 = 0, \tag{A.12}$$

$$(\mathcal{L}^\dagger - \Lambda_3^* I)\vec{u}_4 = 0, \tag{A.13}$$

$$(\mathcal{L}^\dagger - \Lambda_3^* I)\vec{u}_3 = \vec{u}_4. \tag{A.14}$$

The unconventional naming order is for the sake of getting biorthogonal system. The corresponding left generalized eigenvectors, namely $\vec{u}_1, \vec{u}_2, \vec{u}_4, \vec{u}_3$ are given by

$$\vec{u}_1 = \begin{pmatrix} 1 \\ 1 \\ 0 \\ 0 \end{pmatrix}, \tag{A.15}$$

$$\vec{u}_2 = \begin{pmatrix} (1+\Lambda_2)(4\delta^2 + (2\Lambda_2+1)^2) \\ (1-\Lambda_2)(4\delta^2 + (2\Lambda_2+1)^2) \\ -4d\Lambda_2(2\delta - i(2\Lambda_2+1)) \\ -4d\Lambda_2(2\delta + i(2\Lambda_2+1)) \end{pmatrix}, \tag{A.16}$$

$$\vec{u}_4 = \begin{pmatrix} (1+\Lambda_3)(4\delta^2 + (2\Lambda_3+1)^2) \\ (1-\Lambda_3)(4\delta^2 + (2\Lambda_3+1)^2) \\ -4d\Lambda_3(2\delta - i(2\Lambda_3+1)) \\ -4d\Lambda_3(2\delta + i(2\Lambda_3+1)) \end{pmatrix}, \tag{A.17}$$

$$\vec{u}_3 = \frac{1}{\Lambda_3(4\delta^2 + (2\Lambda_3+1)^3)}(\vec{u}_a + \vec{u}_b), \tag{A.18}$$

where

$$\vec{u}_a = \begin{pmatrix} (2\Lambda_3+1)^4(2\Lambda_3^2-1) - 16\delta^4 \\ -(2\Lambda_3+1)^4(2\Lambda_3^2+1) - 16\delta^4 \\ 0 \\ 0 \end{pmatrix}, \tag{A.19}$$

$$\vec{u}_b = \begin{pmatrix} -8\delta^2(4\Lambda_3^4 + 8\Lambda_3^3 + 7\Lambda_3^2 + 4\Lambda_3 + 1) \\ -8\delta^2(-4\Lambda_3^4 + 8\Lambda_3^3 + 9\Lambda_3^2 + 4\Lambda_3 + 1) \\ 16d\delta\Lambda_3^2((2\Lambda_3 + 1)^2 + 2i\delta) \\ 16d\delta\Lambda_3^2((2\Lambda_3 + 1)^2 - 2i\delta) \end{pmatrix}. \tag{A.20}$$

It can be easily verified that left and right generalized eigenvectors,$\vec{v}_k$ and $\vec{u}_j$ form a biorthogonal system such that $\vec{u}_j^\dagger \vec{v}_k = \delta_{jk}$.

A.2 Third-order exceptional points

For third-order EP, three eigenvalues and eigenvectors coalesce. Two more generalized eigenvectors are needed to complete the eigenspace. The right eigenvalue equation and Jordan chain are given by

$$(\mathcal{L} - \Lambda_1 I)\vec{v}_1 = 0, \tag{A.21}$$
$$(\mathcal{L} - \Lambda_2 I)\vec{v}_2 = 0, \tag{A.22}$$
$$(\mathcal{L} - \Lambda_2 I)\vec{v}_3 = \vec{v}_2, \tag{A.23}$$
$$(\mathcal{L} - \Lambda_2 I)\vec{v}_4 = \vec{v}_3, \tag{A.24}$$

where the eigenvalues are given by equations (3.23) and (3.24). The generalized eigenvectors, $\vec{v}_1, \vec{v}_2, \vec{v}_3, \vec{v}_4$ are given by

$$\vec{v}_1 = \frac{1}{32}\begin{pmatrix} 30 \\ 2 \\ \sqrt{2}(-1 - 3i\sqrt{3}) \\ \sqrt{2}(-1 + 3i\sqrt{3}) \end{pmatrix}, \tag{A.25}$$

$$\vec{v}_2 = \frac{3}{32}\begin{pmatrix} -2 \\ 2 \\ \sqrt{2} - i\sqrt{6} \\ \sqrt{2} + i\sqrt{6} \end{pmatrix}, \tag{A.26}$$

$$\vec{v}_3 = \frac{9}{32}\begin{pmatrix} 0 \\ 0 \\ \sqrt{2}(3 - i\sqrt{3}) \\ \sqrt{2}(3 + i\sqrt{3}) \end{pmatrix}, \tag{A.27}$$

$$\vec{v}_4 = \frac{81}{128}\begin{pmatrix} 2 \\ -2 \\ \sqrt{2}(7 + i\sqrt{3}) \\ \sqrt{2}(7 - i\sqrt{3}) \end{pmatrix}. \tag{A.28}$$

The eigenvalue equation and Jordan chain for left generalized eigenvectors are given by

$$(\mathcal{L}^\dagger - \Lambda_1^* I)\vec{u}_1 = 0, \tag{A.29}$$
$$(\mathcal{L}^\dagger - \Lambda_2^* I)\vec{u}_4 = 0, \tag{A.30}$$
$$(\mathcal{L}^\dagger - \Lambda_2^* I)\vec{u}_3 = \vec{u}_4, \tag{A.31}$$
$$(\mathcal{L}^\dagger - \Lambda_2^* I)\vec{u}_2 = \vec{u}_3. \tag{A.32}$$

The corresponding left generalized eigenvectors, namely $\vec{u}_1, \vec{u}_4, \vec{u}_3, \vec{u}_2$ are given by

$$\vec{u}_1 = \begin{pmatrix} 1 \\ 1 \\ 0 \\ 0 \end{pmatrix}, \tag{A.33}$$
$$\vec{u}_4 = \frac{4}{81} \begin{pmatrix} 1 \\ 5 \\ \sqrt{2} + i\sqrt{6} \\ \sqrt{2} - i\sqrt{6} \end{pmatrix}, \tag{A.34}$$
$$\vec{u}_3 = \frac{2}{27} \begin{pmatrix} -3 \\ -27 \\ -4i\sqrt{6} \\ 4i\sqrt{6} \end{pmatrix}, \tag{A.35}$$
$$\vec{u}_2 = \frac{1}{3} \begin{pmatrix} 0 \\ 20 \\ \sqrt{2} + i\sqrt{6} \\ \sqrt{2} - i\sqrt{6} \end{pmatrix}. \tag{A.36}$$

It can be easily verified that the left and right generalized eigenvectors, $\vec{v}_k$ and $\vec{u}_j$ form a biorthogonal system such that $\vec{u}_j^\dagger \vec{v}_k = \delta_{jk}$.

Appendix B

Analytic solution for one-qubit

B.1 Underdamped

The system exhibits underdamped behavior when $p^3 + q^2 > 0$. This underdamped characteristic can be demonstrated by the following argument. When $p^3 + q^2 > 0$, u and s become real numbers, implying that Λ_3 and Λ_4 are complex numbers while Λ_2 remains a real number. In the context of matrix differential equations, complex eigenvalues always indicate oscillatory behavior in the system. We define these eigenvalues in terms of their real and imaginary parts as

$$\Lambda_3 = \lambda + i\omega, \tag{B.1}$$
$$\Lambda_4 = \lambda - i\omega, \tag{B.2}$$

where $|\lambda|$ represents the decay rate and $|\omega|$ represents the angular frequency of the system. λ and ω take the form

$$\lambda = -\frac{2}{3} + \frac{1}{2}(u - s) \tag{B.3}$$

and

$$\omega = -\frac{\sqrt{3}}{2}(u - s). \tag{B.4}$$

Next, we need to solve for the quantum state in underdamped region. The solution can be written as

$$\vec{\rho}(t) = \vec{v}_1 + f_2 e^{\Lambda_2 t}\vec{v}_2 + (f_3 + ig_3)e^{(\lambda+i\omega)t}\vec{v}_3 + (f_3 - ig_3)e^{(\lambda-i\omega)t}\vec{v}_4, \tag{B.5}$$

where $f_2, f_3, g_3 \in \mathbb{R}$ and $\vec{v}_1, \vec{v}_2, \vec{v}_3, \vec{v}_4$ are given by equations (2.33) and (2.41). For $\vec{\rho}(t)$ to adhere to the conditions of a density matrix, the coefficients must take the form of $(f_3 + ig_3)$ and $(f_3 - ig_3)$. In addition to the representation using a density matrix, quantum states can also be expressed on a Bloch sphere through

components for $x(t)$, $y(t)$, and $z(t)$.

$$x(t) = 2\,\mathrm{Re}[m(t)] \tag{B.6}$$
$$y(t) = 2\,\mathrm{Im}[m(t)] \tag{B.7}$$
$$z(t) = 2a(t) - 1 \tag{B.8}$$

Expressing in term of components of Bloch sphere $x(t), y(t)$ and $z(t)$ and absorbing N_2, N_3, N_4 into $f_2, (f_3 + ig_3), (f_3 - ig_3)$, we have

$$\begin{aligned} x(t) =& x_e + 4f_2\delta(1+\Lambda_2)e^{\Lambda_2 t} - 8\delta e^{\Lambda t}(g_3(1+\Lambda) + f_3\omega)\sin\omega t \\ &+ 8\delta e^{\lambda t}(f_3(1+\Lambda) - g_3\omega)\cos\omega t, \end{aligned} \tag{B.9}$$

$$\begin{aligned} y(t) =& y_e + 2f_2(1+\Lambda_2)(1+2\Lambda_2)e^{\Lambda_2 t} \\ &- 4e^{\lambda t}(g_3((1+2\Lambda)(1+\Lambda) - 2\omega^2) + f_3\omega(3+4\Lambda))\sin\omega t \\ &+ 4e^{\lambda t}(f_3((1+2\Lambda)(1+\Lambda) - 2\omega^2) - g_3\omega(3+4\Lambda))\cos\omega t, \end{aligned} \tag{B.10}$$

$$\begin{aligned} z(t) =& z_e + 4f_2 d(1+2\Lambda_2)e^{\Lambda_2 t} - 8de^{\lambda t}(g_3(1+2\Lambda) + 2f_3\omega)\sin\omega t \\ &+ 8de^{\Lambda t}(f_3(1+2\Lambda) - 2g_3\omega)\cos\omega t. \end{aligned} \tag{B.11}$$

Applying initial condition, x_0, y_0, z_0 at $t = 0$, we have

$$\begin{aligned} f_2 =& \frac{1}{8d\delta((\lambda-\Lambda_2)^2+\omega^2)}(-d(2\delta\Delta y + \Delta x((2\lambda+1)^2 + 4\omega^2)) \\ &+ 2\delta\Delta z((\lambda+1)^2+\omega^2)), \end{aligned} \tag{B.12}$$

$$\begin{aligned} f_3 =& \frac{1}{16d\delta((\lambda-\Lambda_2)^2+\omega^2)}(2d\delta\Delta y + d\Delta x(2\Lambda_2+1)(4\lambda - 2\Lambda_2 + 1) \\ &- 2\delta\Delta z(\Lambda_2+1)(2\lambda - \Lambda_2 + 1)), \end{aligned} \tag{B.13}$$

$$\begin{aligned} g_3 =& \frac{1}{16d\delta\omega((\lambda-\Lambda_2)^2+\omega^2)}(-2d\delta\Delta y(\lambda - \Lambda_2) \\ &+ \Delta z(2\delta(\lambda+1)(\Lambda_2+1)(\lambda-\Lambda_2) - 2\delta(\Lambda_2+1)\omega^2) \\ &- d\Delta x(2\Lambda_2+1)((2\lambda+1)(\lambda-\Lambda_2) - 2\omega^2)). \end{aligned} \tag{B.14}$$

where Δx denotes the difference between the equilibrium state x_e and initial state x_0, $\Delta x = x_e - x_0$ and similarly for Δy and Δz and x_e, y_e, z_e are given by equation (2.34)

B.2 Overdamped

On the other hand, the system exhibits overdamped behavior when $p^3 + q^2 < 0$. This overdamped characteristic can be explained as follows. When $p^3 + q^2 < 0$, u and s become complex conjugate to each other, implying that Λ_2, Λ_3 and Λ_4 are real numbers. This suggests that the damping effect dominates, suppressing any oscillatory behavior in the system. Next, the GKSL equation in equation (2.14) is

a type of matrix differential equation that can be solved readily. In overdamping region, the solution is

$$\vec{\rho}(t) = \vec{v}_1 + f_2 e^{\Lambda_2 t}\vec{v}_2 + f_3 e^{\Lambda_3 t}\vec{v}_3 + f_4 e^{\Lambda_4 t}\vec{v}_4, \tag{B.15}$$

where $f_2, f_3, f_4 \in \mathbb{R}$ and $\vec{v}_1, \vec{v}_2, \vec{v}_3, \vec{v}_4$ are given by equations (2.33) and (2.41). f_2, f_3, f_4 must be real because the violation of the condition for a density matrix would occur if f_1, f_2, and f_3 were complex. Therefore, we can explicitly compute $x(t), y(t)$ and $z(t)$. We have

$$x(t) = x_e + \sum_{j=2}^{4} 4 f_j N_j \delta(1+\Lambda_j) e^{\Lambda_j t}, \tag{B.16}$$

$$y(t) = y_e + \sum_{j=2}^{4} 2 f_j N_j (1+\Lambda_j)(1+2\Lambda_j) e^{\Lambda_j t}, \tag{B.17}$$

$$z(t) = z_e + \sum_{j=2}^{4} 4 f_j N_j d(1+2\Lambda_j) e^{\Lambda_j t}. \tag{B.18}$$

We label initial state as $x_0 \equiv x(0)$ and etc whereas, Δx denotes the difference between the equilibrium state x_e and initial state x_0, $\Delta x = x_e - x_0$ and similarly for Δy and Δz. Using initial condition by assuming $t = 0$, we are able to solve for f_2, f_3 and f_4 as

$$\begin{aligned} f_2 =& \frac{1}{8d\delta N_2(\Lambda_2-\Lambda_3)(\Lambda_2-\Lambda_4)}(-d\Delta x(2\Lambda_3+1)(2\Lambda_4+1) \\ &+ 2\delta\Delta z(\Lambda_3+1)(\Lambda_4+1) - 2d\delta\Delta y), \end{aligned} \tag{B.19}$$

$$\begin{aligned} f_3 =& \frac{1}{8d\delta N_3(\Lambda_2-\Lambda_3)(\Lambda_3-\Lambda_4)}(d\Delta x(2\Lambda_2+1)(2\Lambda_4+1) \\ &- 2\delta\Delta z(\Lambda_2+1)(\Lambda_4+1) + 2d\delta\Delta y), \end{aligned} \tag{B.20}$$

$$\begin{aligned} f_4 =& \frac{1}{8d\delta N_4(\Lambda_2-\Lambda_4)(\Lambda_4-\Lambda_3)}(d\Delta x(2\Lambda_2+1)(2\Lambda_3+1) \\ &- 2\delta\Delta z(\Lambda_2+1)(\Lambda_3+1) + 2d\delta\Delta y). \end{aligned} \tag{B.21}$$

B.3 Second-order exceptional points

Let's explore the analytical solution for the quantum state specifically at the second-order EP. The solution is given by

$$\vec{\rho}(t) = \vec{v}_1 + f_2 e^{\Lambda_2 t}\vec{v}_2 + f_3 e^{\Lambda_3 t}\vec{v}_3 + f_4 e^{\Lambda_3 t}(t\vec{v}_3 + \vec{v}_4), \tag{B.22}$$

where $f_2, f_3, f_4 \in \mathbb{R}$ and $\vec{v}_1, \vec{v}_2, \vec{v}_3, \vec{v}_4$ are generalized eigenvector defined in equations (A.5) to (A.8). We can explicitly compute $x(t), y(t)$ and $z(t)$. We have

$$\begin{aligned} x(t) =& x_e + 4f_2\delta(\Lambda_2+1)N_2e^{\Lambda_2 t} + 4\delta(\Lambda_3+1)N_3e^{\Lambda_3 t}(f_3+f_4t) \\ &- \frac{4}{2\Lambda_3+1}f_4\delta N_3 e^{\Lambda_3 t}, \end{aligned} \tag{B.23}$$

$$\begin{aligned} y(t) =& y_e + 2f_2(\Lambda_2+1)(2\Lambda_2+1)N_2e^{\Lambda_2 t} + 2f_4(2\Lambda_3+1)N_3e^{\Lambda_3 t} \\ &+ 2(\Lambda_3+1)(2\Lambda_3+1)N_3e^{\Lambda_3 t}(f_3+f_4t), \end{aligned} \tag{B.24}$$

$$z(t) = z_e + 4f_2d(2\Lambda_2+1)N_2e^{\Lambda_2 t} + 4d(2\Lambda_3+1)N_3e^{\Lambda_3 t}(f_3+f_4t). \tag{B.25}$$

Applying initial condition, we have

$$f_2 = \frac{1}{8d\delta N_2(\Lambda_2-\Lambda_3)^2}(2\delta\Delta z(\Lambda_3+1)^2 - d(2\delta\Delta y + \Delta x(2\Lambda_3+1)^2)), \tag{B.26}$$

$$\begin{aligned} f_3 =& \frac{1}{8d\delta N_3(2\Lambda_3+1)(\Lambda_2-\Lambda_3)^2}(d(2\Lambda_2+1)(2\delta\Delta y + \Delta x(2\Lambda_3+1)^2) \\ &- 2\delta\Delta z(\Lambda_2+1)(\Lambda_2+2\Lambda_3(\Lambda_3+1)+1)), \end{aligned} \tag{B.27}$$

$$\begin{aligned} f_4 =& \frac{1}{8d\delta N_3(\Lambda_2-\Lambda_3)}(2d\delta\Delta y + d\Delta x(2\Lambda_2+1)(2\Lambda_3+1) \\ &- 2\delta\Delta z(\Lambda_2+1)(\Lambda_3+1)). \end{aligned} \tag{B.28}$$

B.4 Third-order exceptional points

Ultimately, we can resolve the equation for the scenario involving a third-order EP, and the solution is given by

$$\vec{\rho}(t) = \vec{v}_1 + f_2e^{\Lambda_2 t}\vec{v}_2 + f_3e^{\Lambda_2 t}(t\vec{v}_2 + \vec{v}_2^{(1)}) + f_4e^{\Lambda_2 t}(\frac{t^2}{2}\vec{v}_2 + t\vec{v}_2^{(1)} + \vec{v}_2^{(2)}), \tag{B.29}$$

where $f_2, f_3, f_4 \in \mathbb{R}$ and $\vec{v}_1, \vec{v}_2, \vec{v}_3, \vec{v}_4$ are generalized eigenvectors defined in equations (A.25) to (A.28). We can explicitly compute $x(t), y(t)$ and $z(t)$. We have

$$x(t) = x_e + \frac{3}{32\sqrt{2}}(4f_2 + 4f_3(t+9) + f_4(2t^2+36t+189))e^{-\frac{2t}{3}}, \tag{B.30}$$

$$y(t) = y_e - \frac{9}{32\sqrt{6}}(4f_2 + 4f_3(t+3) + f_4(2t(t+6)-27))e^{-\frac{2t}{3}}, \tag{B.31}$$

$$z(t) = z_e + \frac{1}{32}(-12f_2 - 12f_3t - 3f_4(2t^2-27))e^{-\frac{2t}{3}}. \tag{B.32}$$

Applying initial condition, we have

$$f_2 = \frac{1}{3}(-\sqrt{2}\Delta x - \sqrt{6}\Delta y + 10\Delta z), \tag{B.33}$$

$$f_3 = \frac{8}{27}(\sqrt{6}\Delta y - 3\Delta z), \tag{B.34}$$

$$f_4 = -\frac{4}{81}(\sqrt{2}\Delta x + \sqrt{6}\Delta y - 2\Delta z). \tag{B.35}$$

Appendix C

Generalized eigenvectors for two-qubit

C.1 Eigensystem

Similar to one-qubit, the dynamics of the system lies in the eigensystem of Liouvillian superoperator $\mathcal{L}$. The eigenvalues of $\mathcal{L}$ are the same, given by equations (4.13) to (4.17). For completeness, we also work out both the right and left eigenvectors. Mathematically, they must be biorthogonal to each other. The corresponding right eigenvectors for the system are

$$\vec{v}_1 = \begin{pmatrix} 1 \\ 0 \\ 0 \\ 0 \\ 0 \\ 0 \\ 0 \\ 0 \end{pmatrix}, \vec{v}_2 = \begin{pmatrix} 1 \\ -1 \\ -1 \\ 1 \\ 0 \\ 0 \\ 0 \\ 0 \end{pmatrix}, \vec{v}_3 = \begin{pmatrix} 0 \\ 0 \\ 0 \\ 0 \\ 0 \\ 0 \\ 0 \\ 1 \end{pmatrix}, \vec{v}_4 = \begin{pmatrix} 0 \\ 0 \\ 0 \\ 0 \\ 0 \\ 0 \\ 1 \\ 0 \end{pmatrix}, \vec{v}_5 = N_5 \begin{pmatrix} 0 \\ 0 \\ 0 \\ 0 \\ 1 \\ 1 \\ 0 \\ 0 \end{pmatrix}, \tag{C.1}$$

$$\vec{v}_6 = N_6 \begin{pmatrix} -2\eta \\ \eta \\ \eta \\ 0 \\ i \\ -i \\ 0 \\ 0 \end{pmatrix}, \vec{v}_7 = N_7 \begin{pmatrix} -2\kappa \\ \kappa - 2\Lambda_7 - 1 \\ \kappa + 2\Lambda_7 + 1 \\ 0 \\ i\eta\kappa \\ -i\eta\kappa \\ 0 \\ 0 \end{pmatrix}, \vec{v}_8 = N_8 \begin{pmatrix} -2\kappa \\ \kappa - 2\Lambda_8 - 1 \\ \kappa + 2\Lambda_8 + 1 \\ 0 \\ i\eta\kappa \\ -i\eta\kappa \\ 0 \\ 0 \end{pmatrix}, \tag{C.2}$$

whereas the left eigenvectors are

$$\vec{u}_1 = \begin{pmatrix} 1 \\ 1 \\ 1 \\ 1 \\ 0 \\ 0 \\ 0 \\ 0 \end{pmatrix}, \vec{u}_2 = \begin{pmatrix} 0 \\ 0 \\ 0 \\ 1 \\ 0 \\ 0 \\ 0 \\ 0 \end{pmatrix}, \vec{u}_3 = \begin{pmatrix} 0 \\ 0 \\ 0 \\ 0 \\ 0 \\ 0 \\ 0 \\ 1 \end{pmatrix}, \vec{u}_4 = \begin{pmatrix} 0 \\ 0 \\ 0 \\ 0 \\ 0 \\ 0 \\ 1 \\ 0 \end{pmatrix}, \vec{u}_5 = \begin{pmatrix} 0 \\ 0 \\ 0 \\ 0 \\ 1 \\ 1 \\ 0 \\ 0 \end{pmatrix}, \vec{u}_6 = \begin{pmatrix} 0 \\ \eta \\ \eta \\ 2\eta \\ -i \\ i \\ 0 \\ 0 \end{pmatrix}, \quad \text{(C.3)}$$

$$\vec{u}_7 = \begin{pmatrix} 0 \\ \eta^2\kappa^2 \\ (1+\kappa+2\Lambda_7^*)^2 \\ 2\kappa(1+\kappa+2\Lambda_7^*) \\ -i\eta\kappa(1+\kappa+2\Lambda_7^*) \\ i\eta\kappa(1+\kappa+2\Lambda_7^*) \\ 0 \\ 0 \end{pmatrix}, \vec{u}_8 = \begin{pmatrix} 0 \\ \eta^2\kappa^2 \\ (1+\kappa+2\Lambda_8^*)^2 \\ 2\kappa(1+\kappa+2\Lambda_8^*) \\ -i\eta\kappa(1+\kappa+2\Lambda_8^*) \\ i\eta\kappa(1+\kappa+2\Lambda_8^*) \\ 0 \\ 0 \end{pmatrix}, \quad \text{(C.4)}$$

where

$$N_5 = \frac{1}{2}, \quad \text{(C.5)}$$

$$N_6 = \frac{1}{2(-1+\eta^2)}, \quad \text{(C.6)}$$

$$N_7 = \frac{1}{(1+\kappa+2\Lambda_7)^3 - \eta^2\kappa^2(3+\kappa+6\Lambda_7)}, \quad \text{(C.7)}$$

$$N_6 = \frac{1}{(1+\kappa+2\Lambda_8)^3 - \eta^2\kappa^2(3+\kappa+6\Lambda_8)}. \quad \text{(C.8)}$$

C.2 Exceptional points of two-qubit system

The structure of the eigensystem for two-qubit system are slightly different from one-qubit system. For system with jump and without jump, they exhibit only third-order EP without exhibiting second-order EP. Third-order EP occurs when $\eta = \pm 1$, the system is in underdamped when $\eta > 1, \eta < -1$ and overdamped when $-1 < \eta < 1$, if we allow η to be negative.

At the EP, the generalized eigenvectors must be used to describe the system

properly. When $\eta = \pm 1$, the right generalized eigenvectors are

$$\vec{v}_6 = N_6 \begin{pmatrix} \mp 2 \\ \pm 1 \\ \pm 1 \\ 0 \\ i \\ -i \\ 0 \\ 0 \end{pmatrix}, \vec{v}_7 = \frac{1}{\kappa} \begin{pmatrix} \mp 2\alpha_3\kappa \\ \pm(-2N_6 + \alpha_3\kappa) \\ \pm(2N_6 + \alpha_3\kappa) \\ 0 \\ i\alpha_3\kappa \\ -i\alpha_3\kappa \\ 0 \\ 0 \end{pmatrix}, \tag{C.9}$$

$$\vec{v}_8 = \frac{1}{\kappa^2} \begin{pmatrix} \pm(-8N_6 - 2\alpha_2\kappa^2) \\ \pm(4N_6 - 2\alpha_3\kappa + \alpha_2\kappa^2) \\ \pm(4N_6 + 2\alpha_3\kappa + \alpha_2\kappa^2) \\ 0 \\ \kappa^2(\alpha_1 + i\alpha_2) \\ \kappa^2(\alpha_1 - i\alpha_2) \\ 0 \\ 0 \end{pmatrix}, \tag{C.10}$$

and left generalized eigenvectors are

$$\vec{u}_8 = \begin{pmatrix} 0 \\ \pm 1 \\ \pm 1 \\ \pm 2 \\ -i \\ i \\ 0 \\ 0 \end{pmatrix}, \vec{u}_7 = \frac{1}{\kappa} \begin{pmatrix} 0 \\ \pm(-2 + \beta_3\kappa) \\ \pm(2 + \beta_3\kappa) \\ \pm 2\beta_3\kappa \\ -i\beta_3\kappa \\ i\beta_3\kappa \\ 0 \\ 0 \end{pmatrix}, \tag{C.11}$$

$$\vec{u}_6 = \frac{1}{\kappa^2} \begin{pmatrix} 0 \\ \pm(4 - 2\beta_3\kappa + \beta_2\kappa^2) \\ \pm(4 + 2\beta_3\kappa + \beta_2\kappa^2) \\ \pm(8 + 2\beta_2\kappa^2) \\ \kappa^2(\beta_1 - i\beta_2) \\ \kappa^2(\beta_1 + i\beta_2) \\ 0 \\ 0 \end{pmatrix}, \tag{C.12}$$

where the following condition is a must to achieve biorthogonality, $\vec{u}_j^\dagger \vec{v}_k = \delta_{jk}$,

$$N_6 = \frac{\kappa^2}{8}, \tag{C.13}$$

$$\beta_3 = -\frac{8\alpha_3}{\kappa^2}, \tag{C.14}$$

$$\beta_2 = \frac{64\alpha_3^2}{\kappa^4} - \frac{8\alpha_2 + 4}{\kappa^2}. \tag{C.15}$$

Appendix D

Analytic solution for two-qubit

D.1 Solution of initial state: $\rho_\Psi(\theta, p)$

For initial state of $\rho_\Psi(\theta, p)$, the solution of density matrix components are

$$d(t) = -\frac{1}{4}(p-1)e^{-t}, \tag{D.1}$$

$$\begin{aligned} a(t) =& -\frac{\eta(\eta + p\sin(\theta)) - (\eta p\sin(\theta)+1)\cosh\left(\frac{1}{2}\sqrt{1-\eta^2}\kappa t\right)}{\eta^2-1}e^{-\frac{t}{2}} \\ &+ d(t) + 1, \end{aligned} \tag{D.2}$$

$$\begin{aligned} b(t) =& \frac{\sqrt{1-\eta^2}(\eta p\sin(\theta)+1)\sinh\left(\frac{1}{2}\sqrt{1-\eta^2}\kappa t\right)}{2(\eta^2-1)}e^{-\frac{t}{2}} \\ &+ \frac{1}{2}(1-a(t)-d(t)), \end{aligned} \tag{D.3}$$

$$\begin{aligned} c(t) =& -\frac{\sqrt{1-\eta^2}(\eta p\sin(\theta)+1)\sinh\left(\frac{1}{2}\sqrt{1-\eta^2}\kappa t\right)}{2(\eta^2-1)}e^{-\frac{t}{2}} \\ &+ \frac{1}{2}(1-a(t)-d(t)), \end{aligned} \tag{D.4}$$

$$\begin{aligned} m(t) =& -\frac{-\eta - p\sin(\theta) + \eta(\eta p\sin(\theta)+1)\cosh\left(\frac{1}{2}\sqrt{1-\eta^2}\kappa t\right)}{2(\eta^2-1)}ie^{-\frac{t}{2}} \\ &+ \frac{1}{2}pe^{-\frac{t}{2}}\cos(\theta), \end{aligned} \tag{D.5}$$

$$h(t) = 0. \tag{D.6}$$

The components of concurrence can be computed as

$$C_1(t) = 2(|m(t)| - \sqrt{a(t)d(t)}), \tag{D.7}$$

$$C_2(t) = -2\sqrt{b(t)c(t)}. \tag{D.8}$$

It follows that the concurrence of the system is

$$C(t) = \max(C_1(t), C_2(t), 0) = C_1(t). \tag{D.9}$$

D.2 Solution of initial state: $\rho_\Phi(\theta, p)$

For initial state of $\rho_\Phi(\theta, p)$, the solution of density matrix components are

$$d(t) = \frac{1}{4}(p+1)e^{-t}, \tag{D.10}$$

$$a(t) = -\frac{\eta^2 - \cosh\left(\frac{1}{2}\sqrt{1-\eta^2}\kappa t\right)}{\eta^2 - 1}e^{-\frac{t}{2}} + d(t) + 1, \tag{D.11}$$

$$b(t) = \frac{\sqrt{1-\eta^2}\sinh\left(\frac{1}{2}\sqrt{1-\eta^2}\kappa t\right)}{2(\eta^2-1)}e^{-\frac{t}{2}} + \frac{1}{2}(1 - a(t) - d(t)), \tag{D.12}$$

$$c(t) = -\frac{\sqrt{1-\eta^2}\sinh\left(\frac{1}{2}\sqrt{1-\eta^2}\kappa t\right)}{2(\eta^2-1)}e^{-\frac{t}{2}} + \frac{1}{2}(1 - a(t) - d(t)), \tag{D.13}$$

$$m(t) = -\frac{i\eta\sinh^2(\frac{1}{4}\sqrt{1-\eta^2}\kappa t)}{\eta^2-1}e^{-\frac{t}{2}}, \tag{D.14}$$

$$h(t) = \frac{1}{2}pe^{-\frac{t}{2}+i\theta}. \tag{D.15}$$

The components of concurrence is given by

$$C_1(t) = \frac{2|\eta|\sinh^2(\frac{1}{4}\sqrt{1-\eta^2}\kappa t)}{|\eta^2-1|}e^{-\frac{t}{2}} - 2\sqrt{a(t)d(t)}, \tag{D.16}$$

$$C_2(t) = pe^{-\frac{t}{2}} - \sqrt{(a(t)+d(t)-1)^2 + \frac{\sinh^2(\frac{1}{2}\sqrt{1-\eta^2}\kappa t)}{\eta^2-1}e^{-t}}. \tag{D.17}$$

It follows that the concurrence of the system is

$$C(t) = \max(C_1(t), C_2(t), 0). \tag{D.18}$$

When $p > 1/3$, the concurrence of the system makes use of both $C_1(t)$ and $C_2(t)$. For $p \leq 1/3$, the concurrence of the system only uses $C_1(t)$ to describe the system.

Bibliography

[1] M. A. Nielsen and I. L. Chuang, *Quantum computation and quantum information: 10th anniversary edition* (Cambridge University Press, 2010).

[2] C. L. Degen, F. Reinhard, and P. Cappellaro, "Quantum sensing", Rev. Mod. Phys. **89**, 035002 (2017).

[3] H.-P. Breuer and F. Petruccione, *The theory of open quantum systems* (Oxford University Press, Jan. 2007).

[4] V. Gorini and A. Kossakowski, "N-level system in contact with a singular reservoir", J. Math. Phys. **17**, 1298–1305 (1976).

[5] V. Gorini, A. Frigerio, M. Verri, A. Kossakowski, and E. Sudarshan, "Properties of quantum markovian master equations", Rep. Math. Phys. **13**, 149–173 (1978).

[6] G. Lindblad, "On the generators of quantum dynamical semigroups", Commun. Math. Phys. **48**, 119–130 (1976).

[7] M. V. Berry, "Physics of nonhermitian degeneracies", Czechoslov. J. Phys. **54**, 1039–1047 (2004).

[8] N. Moiseyev, *Non-hermitian quantum mechanics* (Cambridge University Press, 2011).

[9] W. D. Heiss, "The physics of exceptional points", J. Phys. A: Math. Theor. **45**, 444016 (2012).

[10] K. Ding, C. Fang, and G. Ma, "Non-hermitian topology and exceptional-point geometries", Nat. Rev. Phys. **4**, 745–760 (2022).

[11] N. Zhang, S. Liu, K. Wang, Z. Gu, M. Li, N. Yi, S. Xiao, and Q. Song, "Single nanoparticle detection using far-field emission of photonic molecule around the exceptional point", Sci. Rep. **5**, 11912 (2015).

[12] J. Ren, H. Hodaei, G. Harari, A. U. Hassan, W. Chow, M. Soltani, D. Christodoulides, and M. Khajavikhan, "Ultrasensitive micro-scale parity-time-symmetric ring laser gyroscope", Opt. Lett. **42**, 1556–1559 (2017).

[13] W. Chen, Ş. Kaya Özdemir, G. Zhao, J. Wiersig, and L. Yang, "Exceptional points enhance sensing in an optical microcavity", Nature **548**, 192–196 (2017).

[14] H. Hodaei, A. U. Hassan, S. Wittek, H. Garcia-Gracia, R. El-Ganainy, D. N. Christodoulides, and M. Khajavikhan, "Enhanced sensitivity at higher-order exceptional points", Nature **548**, 187–191 (2017).

[15] P.-Y. Chen, M. Sakhdari, M. Hajizadegan, Q. Cui, M. M.-C. Cheng, R. El-Ganainy, and A. Alù, "Generalized parity-time symmetry condition for enhanced sensor telemetry", Nat. Electron. **1**, 297–304 (2018).

[16] Z.-P. Liu, J. Zhang, Ş. K. Özdemir, B. Peng, H. Jing, X.-Y. Lü, C.-W. Li, L. Yang, F. Nori, and Y.-x. Liu, "Metrology with $\mathcal{PT}$-symmetric cavities: enhanced sensitivity near the $\mathcal{PT}$-phase transition", Phys. Rev. Lett. **117**, 110802 (2016).

[17] H.-K. Lau and A. A. Clerk, "Fundamental limits and non-reciprocal approaches in non-hermitian quantum sensing", Nat. Commun. **9**, 4320 (2018).

[18] J. B. Altepeter, P. G. Hadley, S. M. Wendelken, A. J. Berglund, and P. G. Kwiat, "Experimental investigation of a two-qubit decoherence-free subspace", Phys. Rev. Lett. **92**, 147901 (2004).

[19] Q. Zhang, A. Goebel, C. Wagenknecht, Y.-A. Chen, B. Zhao, T. Yang, A. Mair, J. Schmiedmayer, and J.-W. Pan, "Experimental quantum teleportation of a two-qubit composite system", Nat. Phys. **2**, 678–682 (2006).

[20] H. Jing, Ş. Özdemir, H. Lü, and F. Nori, "High-order exceptional points in optomechanics", Sci. Rep. **7**, 3386 (2017).

[21] S. M. Zhang, X. Z. Zhang, L. Jin, and Z. Song, "High-order exceptional points in supersymmetric arrays", Phys. Rev. A **101**, 033820 (2020).

[22] I. I. Arkhipov, F. Minganti, A. Miranowicz, and F. Nori, "Generating high-order quantum exceptional points in synthetic dimensions", Phys. Rev. A **104**, 012205 (2021).

[23] Z.-Z. Li, W. Chen, M. Abbasi, K. W. Murch, and K. B. Whaley, "Speeding up entanglement generation by proximity to higher-order exceptional points", Phys. Rev. Lett. **131**, 100202 (2023).

[24] S. Chakraborty and A. K. Sarma, "Delayed sudden death of entanglement at exceptional points", Phys. Rev. A **100**, 063846 (2019).

[25] S. Hill and W. K. Wootters, "Entanglement of a pair of quantum bits", Phys. Rev. Lett. **78**, 5022–5025 (1997).

[26] W. K. Wootters, "Entanglement of formation of an arbitrary state of two qubits", Phys. Rev. Lett. **80**, 2245–2248 (1998).

[27] P. W. Shor, "Polynomial-time algorithms for prime factorization and discrete logarithms on a quantum computer", SIAM J. Comput. **26**, 1484–1509 (1997).

[28] N. Gisin, G. Ribordy, W. Tittel, and H. Zbinden, "Quantum cryptography", Rev. Mod. Phys. **74**, 145–195 (2002).

[29] S. Pirandola, U. L. Andersen, L. Banchi, M. Berta, D. Bunandar, R. Colbeck, D. Englund, T. Gehring, C. Lupo, C. Ottaviani, J. L. Pereira, M. Razavi, J. S. Shaari, M. Tomamichel, V. C. Usenko, G. Vallone, P. Villoresi, and P. Wallden, "Advances in quantum cryptography", Adv. Opt. Photonics **12**, 1012–1236 (2020).

[30] I. R. Senitzky, "Dissipation in quantum mechanics. the two-level system", Phys. Rev. **131**, 2827–2838 (1963).

[31] I. R. Senitzky, "Dissipation in quantum mechanics. two-level system. ii", Phys. Rev. **134**, A816–A823 (1964).

[32] F. Bloch, "Nuclear induction", Phys. Rev. **70**, 460–474 (1946).

[33] Y. Tanimura and R. Kubo, "Time-dependent spectrum of a two-level system coupled to a heat bath driven by pulsed laser", J. Phys. Soc. Jpn. **58**, 3001–3012 (1989).

[34] N. Hatano, "Exceptional points of the lindblad operator of a two-level system", Mol. Phys. **117**, 2121–2127 (2019).

[35] D. C. Brody, "Biorthogonal quantum mechanics", J. Phys. A: Math. Theor. **47**, 035305 (2013).

[36] C. M. Bender and S. Boettcher, "Real spectra in non-hermitian hamiltonians having $\mathcal{PT}$ symmetry", Phys. Rev. Lett. **80**, 5243–5246 (1998).

[37] A. Bohm, S. Maxson, M. Loewe, and M. Gadella, "Quantum mechanical irreversibility", Phys. A: Stat. Mech. Appl. **236**, 485–549 (1997).

[38] W. D. Heiss, M. Müller, and I. Rotter, "Collectivity, phase transitions, and exceptional points in open quantum systems", Phys. Rev. E **58**, 2894–2901 (1998).

[39] D. Dast, D. Haag, H. Cartarius, and G. Wunner, "Quantum master equation with balanced gain and loss", Phys. Rev. A **90**, 052120 (2014).

[40] K. Hashimoto, K. Kanki, S. Garmon, S. Tanaka, and T. Petrosky, "On the effect of exceptional points in the Liouvillian dynamics of a 1D quantum Lorentz gas", Prog. Theor. Exp. Phys. **2016**, 053A02 (2016).

[41] F. Minganti, A. Miranowicz, R. W. Chhajlany, I. I. Arkhipov, and F. Nori, "Hybrid-liouvillian formalism connecting exceptional points of non-hermitian hamiltonians and liouvillians via postselection of quantum trajectories", Phys. Rev. A **101**, 062112 (2020).

[42] J. Wiersig, "Robustness of exceptional-point-based sensors against parametric noise: the role of hamiltonian and liouvillian degeneracies", Phys. Rev. A **101**, 053846 (2020).

[43] I. I. Arkhipov, A. Miranowicz, F. Minganti, and F. Nori, "Liouvillian exceptional points of any order in dissipative linear bosonic systems: coherence functions and switching between $\mathcal{PT}$ and anti-$\mathcal{PT}$ symmetries", Phys. Rev. A **102**, 033715 (2020).

[44] P. M. Visser and G. Nienhuis, "Solution of quantum master equations in terms of a non-hermitian hamiltonian", Phys. Rev. A **52**, 4727–4736 (1995).

[45] F. Minganti, A. Miranowicz, R. W. Chhajlany, and F. Nori, "Quantum exceptional points of non-hermitian hamiltonians and liouvillians: the effects of quantum jumps", Phys. Rev. A **100**, 062131 (2019).

[46] J. Wiersig, "Enhancing the sensitivity of frequency and energy splitting detection by using exceptional points: application to microcavity sensors for single-particle detection", Phys. Rev. Lett. **112**, 203901 (2014).

[47] J. Wiersig, "Sensors operating at exceptional points: general theory", Phys. Rev. A **93**, 033809 (2016).

[48] M.-A. Miri and A. Alù, "Exceptional points in optics and photonics", Science **363**, eaar7709 (2019).

[49] L. Feng, X. Zhu, S. Yang, H. Zhu, P. Zhang, X. Yin, Y. Wang, and X. Zhang, "Demonstration of a large-scale optical exceptional point structure", Opt. Express **22**, 1760–1767 (2014).

[50] R. Bronson, *Matrix methods: an introduction* (Gulf Professional Publishing, 1991).

[51] E. Hernández, A. Jáuregui, and A. Mondragón, "Jordan blocks and gamow-jordan eigenfunctions associated with a degeneracy of unbound states", Phys. Rev. A **67**, 022721 (2003).

[52] J. B. Parker and I. Joseph, "Quantum phase estimation for a class of generalized eigenvalue problems", Phys. Rev. A **102**, 022422 (2020).

[53] J. Zhang, Y.-L. Zhou, Y. Zuo, H. Zhang, P.-X. Chen, H. Jing, and L.-M. Kuang, "Exceptional entanglement and quantum sensing with a parity-time-symmetric two-qubit system", Adv. Quantum Technol. **7**, 2300350 (2024).

[54] T. Shi, V. Smirnov, K. Shi, and W. Zhang, "Enhanced response at exceptional points in multiqubit systems for sensing", Phys. Rev. A **111**, 032203 (2025).

[55] A. I. Pavlov, Y. Gefen, and A. Shnirman, "Topological transitions in quantum jump dynamics: hidden exceptional points", Phys. Rev. B **111**, 104301 (2025).

[56] V. Popkov, C. Presilla, and M. Salerno, "Manifolds of exceptional points and effective zeno limit of an open two-qubits system", Phys. Rev. A **111**, L050202 (2025).

[57] E. Schrödinger, "Discussion of probability relations between separated systems", Math. Proc. Camb. Philos. Soc. **31**, 555–563 (1935).

[58] A. Einstein, B. Podolsky, and N. Rosen, "Can quantum-mechanical description of physical reality be considered complete?", Phys. Rev. **47**, 777–780 (1935).

[59] A. Barenco, C. H. Bennett, R. Cleve, D. P. DiVincenzo, N. Margolus, P. Shor, T. Sleator, J. A. Smolin, and H. Weinfurter, "Elementary gates for quantum computation", Phys. Rev. A **52**, 3457–3467 (1995).

[60] A. Peres, "Separability criterion for density matrices", Phys. Rev. Lett. **77**, 1413–1415 (1996).

[61] C. H. Bennett, D. P. DiVincenzo, J. A. Smolin, and W. K. Wootters, "Mixed-state entanglement and quantum error correction", Phys. Rev. A **54**, 3824–3851 (1996).

[62] C. H. Bennett, G. Brassard, S. Popescu, B. Schumacher, J. A. Smolin, and W. K. Wootters, "Purification of noisy entanglement and faithful teleportation via noisy channels", Phys. Rev. Lett. **76**, 722–725 (1996).

[63] P. Horodecki, "Separability criterion and inseparable mixed states with positive partial transposition", Phys. Lett. A **232**, 333–339 (1997).

[64] D. Bruß, "Characterizing entanglement", J. Math. Phys. **43**, 4237–4251 (2002).

[65] W. H. Zurek, "Decoherence, einselection, and the quantum origins of the classical", Rev. Mod. Phys. **75**, 715–775 (2003).

[66] T. F. Jordan, A. Shaji, and E. C. G. Sudarshan, "Dynamics of initially entangled open quantum systems", Phys. Rev. A **70**, 052110 (2004).

[67] R. Horodecki, P. Horodecki, M. Horodecki, and K. Horodecki, "Quantum entanglement", Rev. Mod. Phys. **81**, 865–942 (2009).

[68] N. Brunner, D. Cavalcanti, S. Pironio, V. Scarani, and S. Wehner, "Bell nonlocality", Rev. Mod. Phys. **86**, 419–478 (2014).

[69] J. I. Cirac, D. Pérez-García, N. Schuch, and F. Verstraete, "Matrix product states and projected entangled pair states: concepts, symmetries, theorems", Rev. Mod. Phys. **93**, 045003 (2021).

[70] T. Yu and J. H. Eberly, "Evolution from entanglement to decoherence of bipartite mixed "x" states", Quantum Inf. Comput. **7**, 459–468 (2007).

[71] M. O. T. Cunha, "The geometry of entanglement sudden death", New J. Phys. **9**, 237 (2007).

[72] M. Ali, G. Alber, and A. R. P. Rau, "Manipulating entanglement sudden death of two-qubit x-states in zero- and finite-temperature reservoirs", J. Phys. B: At. Mol. Opt. Phys. **42**, 025501 (2008).

[73] J.-H. An, S.-J. Wang, and H.-G. Luo, "Entanglement dynamics of qubits in a common environment", Phys. A: Stat. Mech. Appl. **382**, 753–764 (2007).

[74] A. Kumar, K. W. Murch, and Y. N. Joglekar, "Maximal quantum entanglement at exceptional points via unitary and thermal dynamics", Phys. Rev. A **105**, 012422 (2022).

[75] S. Daryanoosh, B. Q. Baragiola, T. Guff, and A. Gilchrist, "Quantum master equations for entangled qubit environments", Phys. Rev. A **98**, 062104 (2018).

[76] R. F. Werner, "Quantum states with einstein-podolsky-rosen correlations admitting a hidden-variable model", Phys. Rev. A **40**, 4277–4281 (1989).

[77] J. Lee and M. S. Kim, "Entanglement teleportation via werner states", Phys. Rev. Lett. **84**, 4236–4239 (2000).

[78] T. Hiroshima and S. Ishizaka, "Local and nonlocal properties of werner states", Phys. Rev. A **62**, 044302 (2000).

[79] J. Du, J. Zhu, M. Shi, X. Peng, and D. Suter, "Experimental observation of a topological phase in the maximally entangled state of a pair of qubits", Phys. Rev. A **76**, 042121 (2007).

[80] T.-J. Liu, C.-Y. Wang, J. Li, and Q. Wang, "Experimental preparation of an arbitrary tunable werner state", EPL **119**, 14002 (2017).

[81] D. Jiang, C. Zhai, Y. Song, Z. Peng, J. Yuan, S. Tang, and W. Lu, "Generating bell states and werner states of two qubits via optical field", Phys. Scr. **99**, 055109 (2024).

[82] B. A. Tay and Y. S. H'ng, "Entanglement generation across exceptional points in two-qubit open quantum system: the role of initial states", accepted by Phys. Rev. E (2025).

[83] P.-R. Han, F. Wu, X.-J. Huang, H.-Z. Wu, C.-L. Zou, W. Yi, M. Zhang, H. Li, K. Xu, D. Zheng, H. Fan, J. Wen, Z.-B. Yang, and S.-B. Zheng, "Exceptional entanglement phenomena: non-hermiticity meeting nonclassicality", Phys. Rev. Lett. **131**, 260201 (2023).

[84] Y. S. H'ng and B. A. Tay, "Impacts of local phase on the entanglement dynamics of two-qubit open quantum system", submitted (2025).

[85] J. F. Yang and H. Z. Shen, "Exceptional-point-engineered dispersive readout of a driven three-level atom weakly interacting with coupled cavities in non-markovian environments", Phys. Rev. A **109**, 053712 (2024).

[86] J.-D. Lin, P.-C. Kuo, N. Lambert, A. Miranowicz, F. Nori, and Y.-N. Chen, "Non-markovian quantum exceptional points", Nat. Commun. **16**, 1289 (2025).